NATIONAL ADVISORY COMMITTEE FOR AERONAUTICS

TECHNICAL NOTE 2649

EFFECT OF MACH NUMBER ON THE FLOW AND APPLICATION OF

COMPRESSIBILITY CORRECTIONS IN A TWO-DIMENSIONAL

SUBSONIC-TRANSONIC COMPRESSOR CASCADE HAVING

VARIED POROUS-WALL SUCTION AT THE BLADE TIPS

By William B. Briggs

Lewis Flight Propulsion Laboratory
Cleveland, Ohio

NACA

Washington
March 1952

LD

2472

EFFECT OF MACH NUMBER ON THE FLOW AND APPLICATION OF

COMPRESSIBILITY CORRECTIONS IN A TWO-DIMENSIONAL

SUBSONIC-TRANSONIC COMPRESSOR CASCADE HAVING

VARIED POROUS-WALL SUCTION AT THE BLADE TIPS

By William B. Briggs

SUMMARY

A cascade of 65-(12)10 compressor blades was tested at one geometric setting over a range of inlet Mach number from 0.12 to 0.89. Two groups of data are presented and compared: the first from the cascade operating conventionally with no boundary-layer control, and the second with the boundary layer controlled by a combination of upstream slot suction and porous-wall suction at the blade tips. A criterion for two-dimensionality was used to specify the degree of boundary-layer control by suction to be applied. The data are presented and an analysis is made to show the effect of Mach number on turning angle, blade wake, pressure distribution about the blade profile, and static-pressure rise. The influence of boundary-layer control on these parameters as well as on the secondary losses is illustrated. A system of correlating the measured static-pressure rise through the cascade with the theoretical isentropic values is presented which gives good agreement with the data. The pressure distribution about the blade profile for an inlet Mach number of 0.21 is corrected with the Prandtl-Glauert, Kármán-Tsien, and vector-mean velocity - contraction coefficient compressibility correction factors to inlet Mach numbers of 0.6 and 0.7. The resulting curves are compared with the experimental pressure distributions for inlet Mach numbers of 0.6 and 0.7 so that the validity of applying the three corrections can be evaluated.

INTRODUCTION

Previous investigations have shown the feasibility of using high subsonic inlet Mach numbers to achieve greater stage pressure ratios and mass flows when the loss in efficiency is not excessive and the flow leaving the blades is not distorted to the detriment of downstream stages.

0

An investigation to promote an understanding of the basic behavior of
the separate variables that are subject to Mach number influence was
undertaken at the NACA Lewis laboratory using the NACA 65-(12)10 com-
pressor blade in a two-dimensional cascade. A clearer indication of
the limiting factors was sought by observing the behavior of the pro-
file pressure distribution, wake, and so forth when the cascade was
well into the transonic region and above the Mach number where blade-
boundary-layer separation occurred. Since the Prandtl-Glauert and
Kármán-Tsien compressibility corrections are theoretically based on
small flow deflections, a measure of the validity of applying them to
cascades having appreciable turning was sought. A third compressibility
correction method was developed.

Fundamental inconsistencies exist in much experimental cascade
data, as pointed out in reference 1. In single-stage and multistage
compressor tests, the stage pressure rise has corresponded satisfac-
torily to the turning angle measured. The pressure rise and coeffi-
cient of lift in the cascade, however, have ordinarily been less than
they should be to correspond to the measured turning angle. Thus it has
been concluded that the coefficient of lift of a blade is less in a
solid-wall cascade than in a conventional rotating compressor. In
order to explain this deficiency and also to obtain blade-profile data
which can be used by theoretical two-dimensional analyses in which the
continuity equation must be satisfied, the porous-wall suction tech-
nique of Erwin and Emery (reference 1) was utilized and extended for
the compressible case. The tests were also carried out conventionally
with no suction so that a comparison to ascertain the influence of
boundary-layer control on the individual variables would be available.
A correlation that accounts for the discrepancy between the pressure
rise and turning angle in a cascade is presented.

DESCRIPTION OF APPARATUS

Cascade tunnel. - The two-dimensional cascade tunnel used in the
present investigation is shown schematically in figure 1. An air
supply at pressures from atmospheric to 40 pounds per square inch gage
was available at the inlet. Behind the outlet valve a reservoir vacuum
of 20 or 26 inches of mercury was available. The test section was
designed with the idea of flexibility foremost in mind. The inlet air
angle, measured between the perpendicular to the cascade axis and the
entering air, could be varied from 0° to 75°. Any practical angle of
attack could be set. A solidity as low as 1/2 using five blades of
3-inch chord at zero stagger could be used. In the investigation
herein, only one configuration was used: σ, 1; β_1, 45°; and
α_1, $16\frac{1}{2}^o$.

The test section with one side-wall disk removed is shown in fig-
ure 2. The blades, having a span-to-chord ratio of 4 and a 3-inch chord,
are seen mounted at a 45° inlet air angle. The center blade had
28 static-pressure holes distributed chordwise about its center line.
The claw total tube, wedge static tube, and total-pressure "wake" rake
were mounted in a survey slot 1/2 chord downstream of the blades. A
similar slot was on the opposite tunnel side wall 1/2 chord upstream.
Two sets of remote-controlled top and bottom flaps were employed. Short
flaps 1 chord in length located immediately upstream of the blades were
adjustable outward to compensate for the converging effect of the bound-
ary layer on the top and bottom walls and to open the outer channels as
needed. The second set was adjustable to match the angle of the leaving
air and thus simulate an infinite cascade.

Boundary-layer control mechanism. - A flush suction slot was incor-
porated into the design of the tunnel 1 chord upstream of the blades,
and porous mesh was placed along the blade tips to permit boundary-
layer control. The flush slot can be seen upstream of the blades in
figure 2. In figure 3 are shown the blades assembled in the porous-
wall manifolds prior to mounting in the tunnel. Metallic walls having
a smooth inner surface were used. The walls initially installed were
unsuitable for they were too porous and the channels could not be uni-
formly controlled. They were replaced by walls having a very small
percent open area that proved satisfactory. Varying amounts of fine
steel wool were compacted behind the porous surface to increase the flow
resistance. This equalized the quantity of air removed through each
channel and prevented recirculation into the low pressure regions on the
convex side of the blades. The behavior of the boundary layer is pre-
sented by figure 4. The keyed lines characterize the variation in thick-
ness that prevails under the influence of the different suction arrange-
ments. The boundary layer grows along the tip walls at an accelerated
rate through the positive pressure gradient in the blade passages. This
convergence of the channel free stream increases the outlet velocity and
decreases the pressure recovered. The action of the flush slot is to
reduce the percentage convergence, but it has little effect on the rate
of growth of the boundary layer downstream of the slot. The porous
suction along the blade tips regulates the degree of convergence or
divergence of the free-stream flow through the blade channels and reduces
the induced secondary flows.

Tunnel calibration. - The tunnel inlet has offset top and bottom
walls which were incorporated into the design to accomodate a range of
inlet air angles. Measurements were made to ascertain the uniformity
of conditions at the test section upstream of the blades resulting from
this type of inlet. It was found that the use of side-wall extentions
into the tank, a honeycomb (cells having a cross-sectional area of 1 sq
in. and 6 in. length formed of 1/16-in.-thick masonite), and additional
top and bottom walls, as shown in figure 1, gave a sufficiently uniform
inlet-velocity distribution. The turbulence level was measured just
upstream of the blades with a single hot wire over a range of Mach
number and a general turbulence level of 1 percent existed.

PROCEDURE

Range of investigation. - The NACA 65-(12)10 blade profile was chosen for this investigation because its characteristics have been widely studied and reported. It was tested at design condition so that the forces present would be sufficiently large to give worthwhile results, yet not at conditions so near stall that the blades would be primarily affected by factors other than the Mach number. These conditions were chosen as 45° inlet air angle, $16\frac{1}{2}^\circ$ angle of attack, and a solidity of 1. Five blades were used. The Reynolds number based on chord was held above 3×10^5 (to keep beyond the range where it affects the blade pressure distribution) on all runs except those at an inlet Mach number M_1 of 0.12, where the Reynolds number was 2.2×10^5. The range for all other tests presented is $3.6 \times 10^5 < R_N < 10.4 \times 10^5$.

Two complete series of tests were conducted over a range of M_1 from 0.12 to 0.89. One series was run using no suction and one, with the suction adjusted to satisfy the criterion for two-dimensionality. The no-suction data provide a comparison with conventional cascades that employ no suction whatsoever. Although the flush slots ahead of the blades and the porous material at the blade ends provide different wall conditions than those present in a tunnel having completely solid walls, their influence is probably negligible because they are submerged in the boundary layer and the tunnel has a span-to-chord ratio of 4. The two-dimensional tests provide blade-section data more representative of actual compressor performance as well as data for analytical purposes.

Criterion for two-dimensionality. - It is not uncommon for the data to differ from those of sundry cascade tunnels which have run tests at identical geometrical settings. The difference is produced by the varying tunnel physical designs such as type of inlet, length of test section inlet to blades, turbulence level, arbitrary quantities of air bled through slots to control the boundary layer, and so forth. It has also been found that the experimental pressure rise from so-called two-dimensional cascades is customarily smaller by a marked amount than the value which theoretically corresponds to the measured turning and smaller than the value indicated by actual compressor operation. For these reasons a criterion was chosen by which the degree of two-dimensionality of cascade tests can be evaluated.

The mathematical error functions of reference 2 evaluate the deviation of the flow solution from two-dimensional by use of the irrotational, momentum, and continuity conditions. It would not be reasonable to attempt to adjust test conditions so that the irrotational or momentum equations are satisfied, for discrepancies must be expected to exist when these concepts are applied to a viscous fluid. Also, both equations involve the solution of contour integrals about the blade profile which would require a prohibitive amount of running time to set a test point. Thus the conditions of continuity on the tunnel center line were the sole measure applied to determine the degree of two-dimensionality.

2472

This technique was different from that of reference 1 wherein the suction of boundary-layer air was adjusted until the conditions upstream and downstream of the blades satisfied the continuity equation and the free-stream total energy was maintained constant. The constant total energy refinement was not included in the definition of two-dimensionality for this investigation because of the greatly increased complexity of steeper pressure gradients and varying density that attend compressible flow. The outlet total pressure used in calculating the outlet velocity was obtained by arithmetically averaging values at 20 survey points on the tunnel center line which covered a complete channel including the wake. For use at higher Mach numbers, compressibility must be taken into account in the form

$$\rho_1 \, V_1 \cos \beta_1 = \rho_2 \, V_2 \cos \beta_2$$

or

$$\rho_1 \, V_{1,a} = \rho_2 \, V_{2,a}$$

(See fig. 5.) (The symbols used herein are defined in appendix A.)

Test procedure. - In setting a test point, the sequence of actions was as follows: When the air was flowing at approximately the desired Mach number, the flaps were adjusted until the wall static pressure 1/2 chord upstream of the blades was uniform parallel to the cascade axis. This was indicative of the flow homogeneity before all the blades. The upstream location was used because it is a higher velocity region than that downstream and hence a more accurate adjustment of the flaps could be made. The boundary layer that builds up along the side walls was then reduced upstream of the blades by adjusting the suction through the side-wall slots. The amount of suction was determined by watching the boundary-layer rakes located a short distance behind the slots and making the best compromise between minimum air removal and minimum boundary-layer thickness. The porous suction along the blade tips was then opened and the survey upstream and downstream conditions were measured. Rapid calculations of the densities and the axial velocities indicated whether more or less blade tip suction was required. Adjustments were continued until continuity was satisfied. Then the data were taken.

The amount of air removed by the combined suction systems to satisfy continuity was fairly constant at 9 percent of the total inlet air for all Mach numbers. The suction systems had insufficient capacity to remove the entire mass of air required to satisfy continuity at inlet Mach numbers greater than 0.6.

RESULTS AND DISCUSSION

Suction Influence on Cascade Performance

Effect on pressure distribution. - The effect of varying the types
and amounts of suction on the pressure distribution about a blade at an
inlet Mach number of 0.4 is illustrated in figure 6. Any increase in
suction proportionately lowers the velocity along the entire concave
surface and along all but the forward 10 percent of the convex surface.
A comparison of the two profiles which have blade-tip suction with the
two that do not shows that it changes the nature of the convex surface.
As is discussed subsequently in more detail, blade-tip suction apparently
has a stabilizing effect on the stagnation point (as indicated in
figs. 11 and 12), restraining it from moving toward the convex surface,
which would increase the pressure coefficient C_p over the nose region.
The area of the curve, which is proportionate to the lift, increases as
the suction is increased until two-dimensionality is reached. Addi-
tional suction beyond this point produces a slight decrease. (The dif-
ference between the no-suction and two-dimensional pressure distribu-
tions at any Mach number can be seen by comparing figs. 11 and 12.)

Effect on total-pressure loss. - Total-pressure surveys were made
1/2 chord downstream of the blades at an inlet Mach number of 0.5 to
evaluate the distribution of the losses through the cascade. In addi-
tion to the no-suction and two-dimensional tests, a run was made using
slot suction only so that a distinction could be made between the con-
tributions of the two suction systems. Lines of constant value of the
loss parameter $(p_{0,1} - p_{0,2})/q_1$ are plotted in figure 7. The quan-
tities $p_{0,1}$ and q_1 are constant free-stream values upstream of the
blades, and $p_{0,2}$ is the local downstream value measured by the survey.
Thus the parameter gives the total deficiency at the outlet including
the inlet boundary-layer losses.

A comparison of the three figures shows the high-loss area decreas-
ing both in extent and intensity as the amount of suction is increased.
Most of the decrease is due to the removal of the inlet boundary layer
by the suction slot. The blade end suction, though, in suppressing the
boundary-layer build-up through the blades (as illustrated in fig. 4),
appreciably diminishes the outlet total-pressure deficiency. The
inclination of the lines is as described in reference 3 for flow around
a bend. As the amount of suction is increased and the greater pressure
rise along the center line imposes a steeper pressure gradient upon the
flow, the inclination of the total-pressure lines increases slightly,
as might be expected.

Mach Number Influence on Cascade Performance

Effect on turning angle. - In figure 8, the turning angle is
plotted against the Mach number as measured with no suction and under
conditions of two-dimensionality. When suction is not used, the mag-
nitude of the turning angle rises approximately $1°$ from an M_1 of 0.12
to 0.7, where it remains fairly constant until M_1 of 0.8, above which
it rapidly diminishes. The two-dimensional tests show the turning angle
to be constant through the range of M_1 below 0.7. Between 0.7 and
0.8, a scatter of $\pm 1/2°$ is seen with the average value diminishing
slightly. Above 0.8 the sharp decrease is the same that occurred at the
no-suction condition.

Effect on lift coefficient. - The theoretical values of coefficient
of lift C_l are plotted on figure 9 to afford a comparison with the
values calculated from the no-suction and two-dimensional data. C_l is
defined by

$$C_l = \frac{2(\Delta V_w)}{\sigma V_m} - C_D \tan \beta_m$$

where

$$C_D = \frac{2 \cos \beta_m}{\sigma V_m}\left[(\Delta V_w) \sin \beta_m - \frac{(p_2 - p_1)}{\rho_m V_m} - (V_{2,a} - V_{1,a}) \cos \beta_m\right]$$

The theoretical values of V_2 are calculated from the continuity
equation and equation (6) of appendix B. The drag coefficient is of
insignificant magnitude at inlet Mach numbers less than 0.85. Above
M_1 of 0.8, separation greatly increases C_D and the turning angle
decreases, so that C_l is rapidly decreased. The two-dimensional data
follow the theoretical curve at M_1 less than 0.6 and then remain con-
stant until M_1 of 0.85, where they drop. The no-suction data follow
a similar trend at approximately nine-tenths the value of the two-
dimensional data.

A plot of the areas enclosed in the curves of figures 11 and 12,
which would be the normal force coefficient perpendicular to the chord
line, shows the same variation.

Effect on blade wake. - The variation of the blade wake, measured
on the tunnel center line, with M_1 is shown in the two plots of fig-
ure 10. The profiles of the wake as measured with total-pressure tubes
1/2 chord length downstream of the trailing edge are presented in fig-
ure 10(a); one plot is for two-dimensional conditions and one is for

no suction. The loss of total pressure is plotted in percent of the difference in outlet free-stream total pressure and outlet static pressure. The magnitude of the wake is changed very little up to M_1 of 0.77 in either case. At M_1 of 0.77, the blade has a peak surface M_1 of 1.16 when operating two-dimensionally and 1.29 with no suction. Notice that the increase in loss occurs principally on the convex surface. The effect of shocks shows up as a pressure deficiency well out into the channel on the convex surface side. The two-dimensional plot (M_1 of 0.77) shows this particularly well.

A cross plot affording a comparison of the two conditions is given in figure 10(b). The difference is slight throughout the range of Mach numbers with the loss consistently larger in the two-dimensional case. As greater diffusion is obtained with two-dimensionality, a stronger positive pressure gradient is imposed on the boundary layer, and the rate of growth is amplified.

Effect on blade pressure distribution. - In order to reduce the confusion of many curves on a single plot, the pressure distributions at M_1 of 0.6 and less are shown in one figure and those for 0.6 and greater in another. The curves for M_1 of 0.12 are presented for comparison although the Reynolds number based on chord is only 2.2×10^5, which is in the range where a Reynolds number distortion of the pressure distribution is possible. In describing variations of the pressure coefficient C_p, the algebraic sense will be used.

(a) Without suction

As is seen in figure 11, the pressure increases over the rear 50 percent of the concave surface as the Mach number increases until separation on the convex surface between M_1 of 0.8 and 0.85 restricts the channel and increases the concave surface velocities. The pressure coefficient C_p over the forward 50 percent of the concave surface diminishes as the inlet Mach number increases to 0.8, where it remains constant. At M_1 of 0.6 and above, the entire concave surface has a positive pressure gradient.

On the convex surface the values of C_p over the rear 40 percent are practically unchanged throughout the range of Mach number where the flow is unseparated. However, over the forward 60 percent, aside from the leading edge, C_p drops rapidly and uniformly as M_1 increases to 0.76. Above this value the oblique shocks become stronger and distort the uniform rate of diffusion by recovering most of the pressure in the region immediately behind the peak C_p point, as shown by the curve for M_1 of 0.8.

The pressure coefficient about the leading edge rises continuously on the convex surface and drops on the concave surface throughout the Mach number range, indicating a shift of the stagnation point toward the convex surface as the Mach number increases. This shift is coincident with the shift of the minimum C_p position on the convex surface from approximately 9 percent chord at M_1 of 0.22 to 31 percent chord at M_1 of 0.8 and greater.

(b) With suction to satisfy two-dimensionality

As seen in figure 12, C_p on the concave surface increases over the entire length as the inlet Mach number increases to 0.61. As the inlet Mach number increases above 0.61, C_p over the forward 50 percent diminishes very slightly and the rear 50 percent is practically unchanged until, between 0.81 and 0.85, separation occurs, restricting the channel and progressively decreasing C_p over the entire surface.

On the convex surface a pivot point appears at the 40-percent-chord point with the local pressure coefficients uniformly decreasing upstream and uniformly increasing downstream as M_1 increases to 0.61. As the peak C_p continues to decrease above M_1 of 0.61 to a minimum at M_1 of 0.81, the oblique shocks are strengthening and rapidly recover pressure just at the start of diffusion so that the local C_p's over the rear area are above the values at M_1 of 0.61. After separation the peak values subside and the C_p over the rear areas decreases.

The local C_p in the leading-edge region rises continuously on the convex surface as the Mach number increases. On the concave surface, C_p rises until M_1 of 0.61 is reached, above which it progressively decreases. The inability of the suction system to remove the entire mass flow required by the two-dimensionality criteria above M_1 of 0.6 possibly permitted the small peaks on the leading 2 percent of the concave surface, which are characteristic of the no-suction profiles, to assert themselves. The position of maximum velocity shifts from 10 percent chord at M_1 of 0.21 to 24 percent chord at M_1 of 0.81, and then back to 20 percent chord at higher Mach numbers.

(c) Comparison

The primary effect of suction is to raise the C_p over the blade surface, as is evident over the entire concave surface and over the convex surface behind the point at 25 percent chord. The stabilization of the stagnation point by suction causes the two-dimensional

curves to have lower C_p values over the forward 25 percent of the convex surface. At the 25-percent-chord position, the two-dimensional profiles have largely passed their convex surface peak velocity, indicating that the main flow is diverging; however, the no-suction profiles have a rising velocity at 25-percent chord, indicating that the side-wall boundary layers are creating a main flow channel that is still converging locally.

The minimum C_p on the blade surface is lower in the two-dimensional case up to M_1 of 0.6, possibly because of the stabilized stagnation point. At M_1 above 0.6, however, the no-suction curves have lower minimum values. The influence of the shifting stagnation point is overcome by a greater convergence of the side-wall boundary layer and the center-line flow reaches a lower peak C_p value. This action suggests that the side-wall boundary layer may separate at the pressure rise imposed on the flow by M_1 above 0.6. There are no measurements to corroborate this.

The effect of the shocks on surface C_p is analytically illustrated by Emmons in reference 4. The C_p plot would theoretically show a large discontinuous algebraic rise through the shock followed by a rapid fall of lesser magnitude. Although surface static-pressure taps are insufficiently sensitive and are ordinarily spaced too far apart to register this complete pattern, evidences of it can be seen, particularly in the curves for M_1 of 0.76. The pronounced inflection of the two-dimensional pressure profile at M_1 of 0.76 has been faired in with a dashed line because the points are insufficient to completely describe the variation of flow.

Effect on static-pressure rise. - In figure 13 the static-pressure rise data are plotted against M_1. Since the suction system of the test rig was unable to remove a mass of air sufficient to satisfy two-dimensionality above M_1 of 0.6, an effort was made to correct the data to achieve a correlation with the theoretically calculated values and to separate the effects of M_1 from the effects of contraction. In each two-dimensional test, an effort was made to keep the contraction coefficient equal to unity, but at the high M_1 where this was impossible, maximum suction was applied and the resulting contraction coefficient was calculated.

The theoretical isentropic values using equation (6) (appendix B) are plotted as a dash-dot line in figure 13. These values deviate from the no-suction data at low M_1 but follow the two-dimensional data to approximately M_1 of 0.55. In order to ascertain the deviation from the theoretical values due to contraction, equation (7) (appendix B)

was plotted as a dashed curve for both conditions using β_1 of 45°, β_2 calculated from the turning angles of figure 8, and the measured values of K. The resulting curve for the two-dimensional case is seen to follow the data very well to M_1 of 0.8.

The curve as corrected for no suction begins deviating at M_1 of 0.5 but follows rather closely to M_1 of 0.8. In spite of the fact that the blades under two-dimensional conditions have greater wake losses (as shown in fig. 10(b)), the difference along the center line between the inlet total pressure and the integrated outlet total pressure is significantly greater in the no-suction condition at high values of M_1. It can be assumed that the secondary losses of large magnitude dissipate total pressure on the cascade center line, causing the no-suction pressure rise to fall below the corrected theoretical. This effect, then, is separate from those effects of contraction and shock losses.

Both curves are seen to break off at a Mach number of 0.8 where the Mach number losses begin to take effect. The peak surface Mach number at M_1 of 0.8 is 1.29 for the two-dimensional case and 1.30 for the no-suction case, and does not rise above these values as M_1 is further increased. It is most interesting to see that blades operating with strong oblique shocks and separated flow on their convex surface will still maintain appreciable loading and produce a large pressure rise. Since the pressure rise is a function of $M_1{}^2$, the plot of pressure rise against M_1 has only a gradual drop from the theoretical value after the M_1 producing separation is exceeded, although the turning angle, coefficient of lift, and efficiency may decrease rapidly.

Application of Compressibility Correction Methods

In figures 14 to 17 the experimental pressure distributions at inlet Mach numbers of approximately 0.6 and 0.7 are compared with the predicted distributions for the same M_1. The predicted curves were obtained by taking as incompressible the experimental distributions at M_1 of 0.21 and applying compressibility corrections by three different methods. The curves for M_1 of 0.21 were used because they are the lowest M_1 curves available at which the Reynolds number is above the range of possible distortion. The maximum blade surface Mach number at M_1 of 0.21 is 0.27, so that the variation of the velocity and the density due to compressibility may be considered to be of a negligible order of magnitude. The manner of applying the Prandtl-Glauert and Kármán-Tsien methods as well as a third that involves the use of the vector-mean velocity - contraction coefficient (V_m and K method) is outlined in appendix C.

When compressibility corrections are applied to a cascade, the predicted values will be not for the same geometric arrangement but for an altogether different one. Woolard points out in reference 5 that, when the blade dimensions are held unchanged, the angle of attack will be unchanged but the inlet air angle β_1 and solidity σ of the cascade to which the predicted distribution corresponds will not be the same as the incompressible one to which the correction is applied. The relations are

$$\left(\alpha_m\right)_c = \left(\alpha_m\right)_i$$

$$\sigma_c = \frac{\sigma_i}{\cos(\beta_m)_i \sqrt{\dfrac{1}{\Omega^2} + \tan^2(\beta_m)_i}}$$

$$\left(\beta_1\right)_c = \left(\alpha_1 - \alpha_m\right) - \operatorname{arc\,cot}\left[\Omega \tan(\beta_m)_i\right] + 90$$

The experimental curves with which the predictions are compared were obtained in every case at a solidity of 1 and a stagger angle of 45°. The values of solidity and stagger angle to which the prediction applies vary with the mean Mach number and are given on each figure. The experimental curve thus serves only as a guide to evaluating the validity of the predicted curves rather than as an absolute criterion with which to compare. The magnitude of the σ and β change is not large, however, and the data are from a range where a small change will have only a slight effect on the aerodynamic parameters. A pointwise comparison could be made only with an experimental curve from a cascade having the values of σ_c and $\beta_{1,c}$ for which the predicted curves apply.

In appraising the usefulness of the three schemes, it is first noted that the solidity and stagger angle are both less in every instance than those for the experimental curve and both changes are in the direction of less turning. The predicted curve then should be expected to have a smaller value of C_l so that its area should be slightly less than that of the experimental curve.

The percentage difference in the areas of the predicted curves and the experimental curve is plotted in figure 18. The method of V_m and K is seen to be the most accurate in this respect with the Prandtl-Glauert and Kármán-Tsien corrections based on the outlet Mach number being second best.

2472

The percentage difference in the predictions for the curves for M_1 of 0.7 is greater than for the curves for M_1 of 0.6 in each case because the presence of supersonic velocities and attendant shocks on the blade surface at a Mach number 0.7 contributes to distortion. On the convex surface, the Prandtl-Glauert and Kármán-Tsien predictions are, in general, good for the no-suction distributions but overcompensate on the two-dimensional distributions. At the same time they are good on the concave surface for the two-dimensional but overcorrect on the no-suction distributions. The V_m and K correction method seems consistently to predict velocities of too small a magnitude. Of course, none of the methods predicts the effect of the stagnation-point shift. In general, the Kármán-Tsien method based on M_1 seems to give the best prediction for the no-suction condition. The nature of diffusion, when two-dimensional suction is used, is much different at M_1 of 0.21 than at M_1 of 0.61 so that the Prandtl-Glauert and Kármán-Tsien corrections overestimate the velocities on the convex surface. A composite curve from the predictions could be made to match the two-dimensional experimental curves, but no single prediction could be recommended.

SUMMARY OF RESULTS

A cascade of 65-(12)10 compressor blades was tested at one geometric setting over a range of inlet Mach number from 0.12 to 0.89. Two groups of data showing the effect of Mach number on aerodynamic parameters are presented and compared: the first from the cascade operating conventionally with no boundary-layer control, and the second with the boundary layer controlled by a combination of upstream slot suction and porous-wall suction at the blade tips. The discrepancy in the measured values of static-pressure rise through the cascade and the theoretical values is correlated by use of the contraction coefficient. The pressure distribution about the blade profile for an inlet Mach number of 0.21 is corrected with the Prandtl-Glauert, Kármán-Tsien, and vector-mean velocity - contraction coefficient compressibility correction factors to inlet Mach numbers of 0.6 and 0.7. The results were as follows:

1. By the use of porous-wall suction along the blade tips, the converging effect of the boundary layer on that wall can be suppressed so that the performance of the aerodynamic parameters measured on the center line closely corresponds to the theoretical values and to the values obtained in rotating cascades. Cascade pressure-rise data that did not agree with theoretical values were correlated at velocities below the Mach number where strong shocks develop by an application of the contraction coefficient. Suction in a cascade having a span-to-chord ratio of 4 had only a small effect on the blade wakes taken on the tunnel center line. However, it reduced the secondary channel losses greatly, both in extent and intensity, and reduced the concomitant total-pressure loss on the tunnel center line.

2. As the inlet Mach number to a cascade was increased, the peak blade pressure coefficient increased in magnitude and shifted rearward in position until a strong shock that produced separation was developed in the channel. With increasing inlet Mach number, the stagnation point moved toward the convex surface of the blade. The use of suction stabilized the stagnation point and decreased the shift of the peak pressure coefficient as the Mach number was increased.

3. Increasing the Mach number in a cascade had an insignificant effect on the blade wake and turning angle until strong shocks developed. A further increase caused the turning angle to drop sharply. These results indicated that if turning angle information alone is desired it is unnecessary to test blade profiles in a high-speed cascade or to employ suction if blades having a span-to-chord ratio of 4 are used.

4. The three compressibility correction methods, when applied to low Mach number experimental pressure distributions, gave reasonably good agreement with the experimental distributions at high Mach number. The Kármán-Tsien method based on inlet Mach number was in closest agreement with the no-suction distributions, the discrepancies being due to the stagnation-point shift for which compressibility corrections do not account.

In order to match the two-dimensional experimental curves, a composite using the predicted concave surface and minimum pressure coefficient value from either the Kármán-Tsien method based on mean Mach number or the Prandtl-Glauert method based on inlet Mach number and the convex-surface diffusion from the vector-mean velocity - contraction coefficient prediction was most accurate. The vector-mean velocity - contraction coefficient predictions most accurately estimated the lift coefficient parameter.

Lewis Flight Propulsion Laboratory
    National Advisory Committee for Aeronautics
        Cleveland, Ohio, December 6, 1951

APPENDIX A

SYMBOLS

The following symbols are used in this report:

C_D drag coefficient

C_p pressure coefficient, $\dfrac{p_b - p_1}{q_1}$

C_l lift coefficient

c   blade chord (ft)

K   contraction coefficient, (center line values) $\dfrac{\rho_1 V_{1,a}}{\rho_2 V_{2,a}}$

M   Mach number

p   static pressure (lb/sq ft)

q   dynamic pressure, $\frac{1}{2} \rho V^2$, (lb/sq ft)

T   stagnation temperature, ($^\circ$R)

V   velocity of air (ft/sec)

α angle between velocity vector and chord line of blades (deg)

β angle between velocity vector and normal to cascade (deg)

γ ratio of specific heats of air

ρ air mass density (slugs/cu ft)

σ solidity, blade chord divided by spacing

φ angle between V_m and tangent to blade profile (deg)

Ω $\sqrt{1 - M_m{}^2}$

Subscripts:

a   axial

b   blade surface

c   compressible

i   incompressible

m   mean, relating to vector mean velocity

p   blade concave surface

u   blade convex surface

w   tangential

O   stagnation condition

1   upstream of cascade

2   downstream of cascade

APPENDIX B

CALCULATION OF THEORETICAL STATIC-PRESSURE CHANGE THROUGH

CASCADE OF BLADES AS FUNCTION OF MACH NUMBER

The energy equation for steady, isentropic flow of air is

$$\frac{V_1^2}{2} + \frac{\gamma}{\gamma-1}\frac{p_1}{\rho_1} = \frac{V_2^2}{2} + \frac{\gamma}{\gamma-1}\frac{p_2}{\rho_2} \tag{1}$$

Transposing and grouping terms give

$$\frac{\gamma-1}{\gamma}\left(\frac{V_1^2 - V_2^2}{2}\right)\frac{\rho_2}{p_1} = \frac{p_2}{p_1} - \frac{\rho_2}{\rho_1} \tag{2}$$

Insertion of the isentropic relation $\frac{\rho_2}{\rho_1} = \left(\frac{p_2}{p_1}\right)^{1/\gamma}$ results in

$$\left(\frac{V_1^2 - V_2^2}{2}\right)(\gamma - 1)\left(\frac{\rho_1}{\gamma p_1}\right)\left(\frac{p_2}{p_1}\right)^{1/\gamma} = \frac{p_2}{p_1} - \left(\frac{p_2}{p_1}\right)^{1/\gamma} \tag{3}$$

$$\frac{\gamma-1}{2}\left[1 - \left(\frac{V_2}{V_1}\right)^2\right]\left(\frac{V_1^2}{\frac{\gamma p_1}{\rho_1}}\right) = \left(\frac{p_2}{p_1}\right)^{\frac{\gamma-1}{\gamma}} - 1 \tag{4}$$

Substituting for $\left(\frac{V_1^2}{\frac{\gamma p_1}{\rho_1}}\right) = M_1^2$ and solving for pressure ratio yield

$$\left(\frac{p_2}{p_1}\right) = \left\{1 + \frac{\gamma-1}{2} M_1^2\left[1 - \left(\frac{V_2}{V_1}\right)^2\right]\right\}^{\frac{\gamma}{\gamma-1}} \tag{5}$$

The continuity equation is used to eliminate the velocities:

$$\frac{V_2}{V_1} = \frac{\rho_1}{\rho_2} \frac{\cos \beta_1}{\cos \beta_2} = \left(\frac{p_1}{p_2}\right)^{1/\gamma} \frac{\cos \beta_1}{\cos \beta_2}$$

Substituting the continuity equation into equation (5) gives

$$\frac{p_2}{p_1} = \left\{ 1 + \frac{\gamma-1}{2} M_1^2 \left[1 - \left(\frac{\cos \beta_1}{\cos \beta_2}\right)^2 \left(\frac{p_1}{p_2}\right)^{2/\gamma} \right] \right\}^{\frac{\gamma}{\gamma-1}} \qquad (6)$$

When the experimental values of β_1 and β_2 are known, equation (6) relates the pressure ratio across the cascade to the M_1 for isentropic flow of a compressible fluid.

The continuity equation will not be satisfied on the center line of a tunnel which has a boundary layer that produces a spanwise contraction of the flow through the blades. Making use of the contraction coefficient

$$K = \frac{\rho_1 V_1 \cos \beta_1}{\rho_2 V_2 \cos \beta_2}$$

gives the theoretical pressure ratio with contraction as

$$\frac{p_2}{p_1} = \left\{ 1 + \frac{(\gamma-1)M_1^2}{2} \left[1 - \frac{1}{K^2} \left(\frac{\cos \beta_1}{\cos \beta_2}\right)^2 \left(\frac{p_1}{p_2}\right)^{2/\gamma} \right] \right\}^{\frac{\gamma}{\gamma-1}} \qquad (7)$$

2472

APPENDIX C

APPLICATION OF COMPRESSIBILITY CORRECTION METHODS TO

INCOMPRESSIBLE PRESSURE DISTRIBUTION FOR PREDICTING

DISTRIBUTION AT COMPRESSIBLE MACH NUMBERS

Prandtl-Glauert and Kármán-Tsien Methods

The applications of the Prandtl-Glauert and Kármán-Tsien methods are quite similar:

Given: $C_{p,i}$ distribution

Choose: M_c for which distribution is desired (In the plots labeled "average Mach number," the arithmetic average of the inlet and outlet values was used.)

Then the Prandtl-Glauert correction of the incompressible pressure coefficient will be

$$C_{p,c} = \frac{C_{p,i}}{\sqrt{1-M_c^2}} \qquad (8)$$

and the Kármán-Tsien correction will be

$$C_{p,c} = \frac{C_{p,i}}{\sqrt{1-M_c^2} + \left(\dfrac{M_c^2}{1+\sqrt{1-M_c^2}}\right)\dfrac{C_{p,i}}{2}} \qquad (9)$$

Vector-Mean Velocity - Contraction Coefficient Method

The method of applying the compressibility correction for a cascade based on the vector mean velocity and using the contraction coefficient is as follows:

Given: $C_{p,i}$ distribution, total temperature T_i, blade profile coordinates, and flow orientation $\left[(V_1)_i, (V_2)_i, \beta_1, \beta_2, \alpha_m\right]$

Choose: $(M_1)_c$, T_c, and $(p_0)_c$ for which a distribution is desired and a contraction coefficient K

Assume: The turning angle is the same as for incompressible flow and ρ is an isentropic function of p.

Calculate the magnitude of the velocity $(V_b)_i$ (from $C_{p,i}$ and T_i) and the direction φ (from profile coordinates and α_m) at various points on the blade surface. Resolve the velocity into components parallel $(V_b)_i \cos \varphi$ and perpendicular v_i to the vector mean velocity $(V_m)_i$. Then the perturbation parallel to the vector mean velocity is

$$u_i = (V_b)_i \cos \varphi - (V_m)_i \qquad (10)$$

Using

$$(V_1)_c = (M_1)_c \left(49 \sqrt{T_c}\right) \qquad (11)$$

obtain $(V_2)_c$ by trial-and-error solution from

$$\frac{V_1}{V_2} = \frac{K \cos \beta_2}{\cos \beta_1} \left\{ 1 + \frac{\gamma-1}{2} (M_1)_c^2 \left[1 - \left(\frac{V_2}{V_1}\right)^2 \right] \right\}^{\frac{1}{\gamma-1}} \qquad (12)$$

Obtain $(V_m)_c$ vectorially from $(V_1)_c$ and $(V_2)_c$ and calculate

$$(M_m)_c = \frac{(V_m)_c}{49 \sqrt{T_c}} \qquad (13)$$

Then

$$u_c = u_i \frac{1}{\sqrt{1-(M_m)_c^2}} \left[\frac{(V_1)_c}{(V_1)_i}\right] \qquad (14)$$

and

$$(V_b)_c = \sqrt{\left[(V_m)_c + u_c\right]^2 + \left\{v_i \left[\frac{(V_1)_c}{(V_1)_i}\right]\right\}^2}$$ (15)

This velocity may be transformed back into the coefficient of pressure by calculating

$$B = \left(\frac{\gamma-1}{2\gamma}\right)\frac{(\rho_0)_c}{(p_0)_c}$$ (16)

and

$$(p_1)_c = (p_0)_c \left[1 - B(V_1)_c^{\,2}\right]^{\frac{\gamma}{\gamma-1}}$$ (17)

then

$$(C_p)_c = \frac{\left[1 - B(V_b)_c^{\,2}\right]^{\frac{\gamma}{\gamma-1}} - \frac{(p_1)_c}{(p_0)_c}}{\left(\frac{\gamma}{\gamma-1}\right)B(V_1)_c^{\,2}\left[\frac{(p_1)_c}{(p_0)_c}\right]^{1/\gamma}}$$ (18)

2472

REFERENCES

1. Erwin, John R., and Emery, James C.: Effect of Tunnel Configuration and Testing Technique on Cascade Performance. NACA Rep. 1016, 1952. (Formerly TN 2028.)

2. Sinnette, John T., Costello, George R., and Cummings, Robert L.: Expressions for Measuring the Accuracy of Approximate Solutions to Compressible Flow Through Cascades of Blades with Examples of Use. NACA TN 2501, 1951.

3. Hawthorne, William R.: Secondary Circulation in Fluid Flow. Gas Turbine Lab., M.I.T., May 1951.

4. Emmons, Howard W.: Flow of a Compressible Fluid past a Symmetrical Airfoil in a Wind Tunnel and in Free Air. NACA TN 1746, 1948.

5. Woolard, Henry W.: A Note on the Subsonic Compressible Flow About Airfoils in a Cascade. Jour. Aero. Sci., vol. 17, no. 6, June 1950, pp. 379-381.
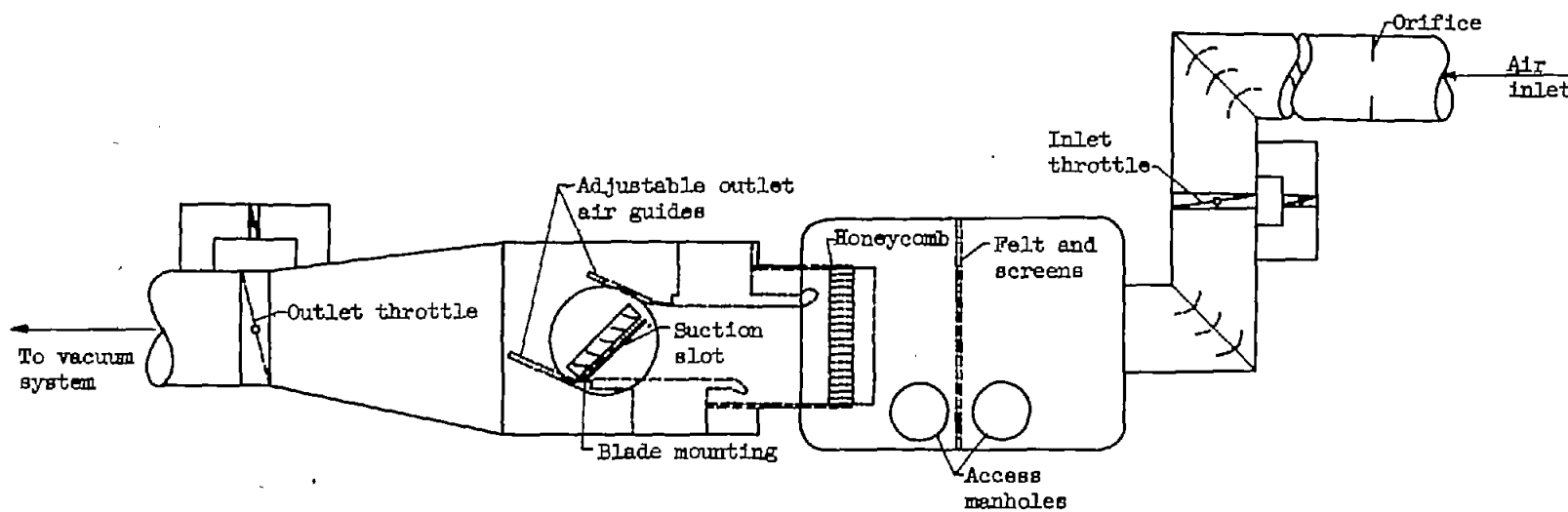
2472

Figure 1. - Schematic diagram of two-dimensional cascade installation.
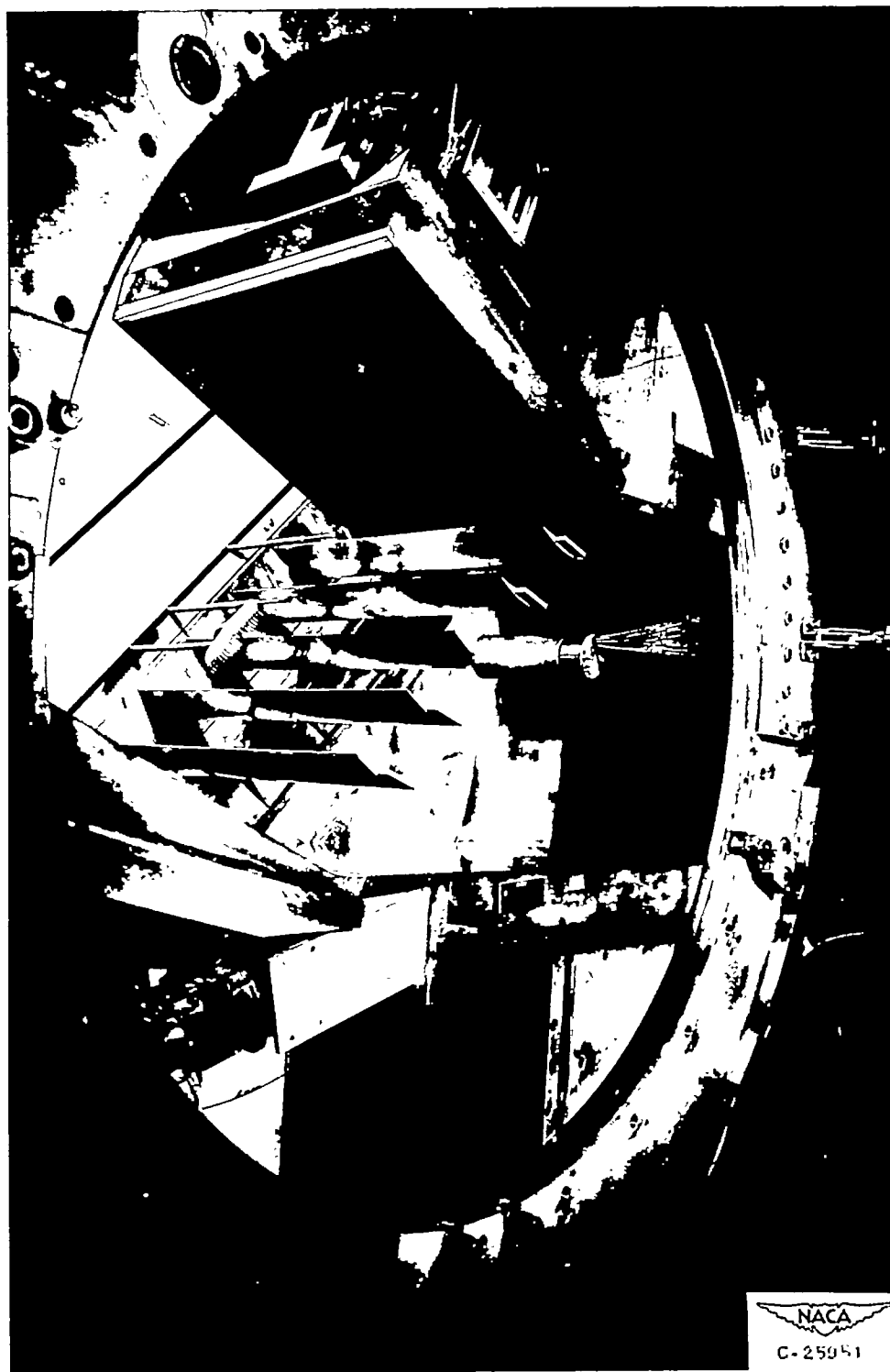
Figure 2. - Test section with one side-wall disk removed to show working arrangement
of components

2472

C-25478
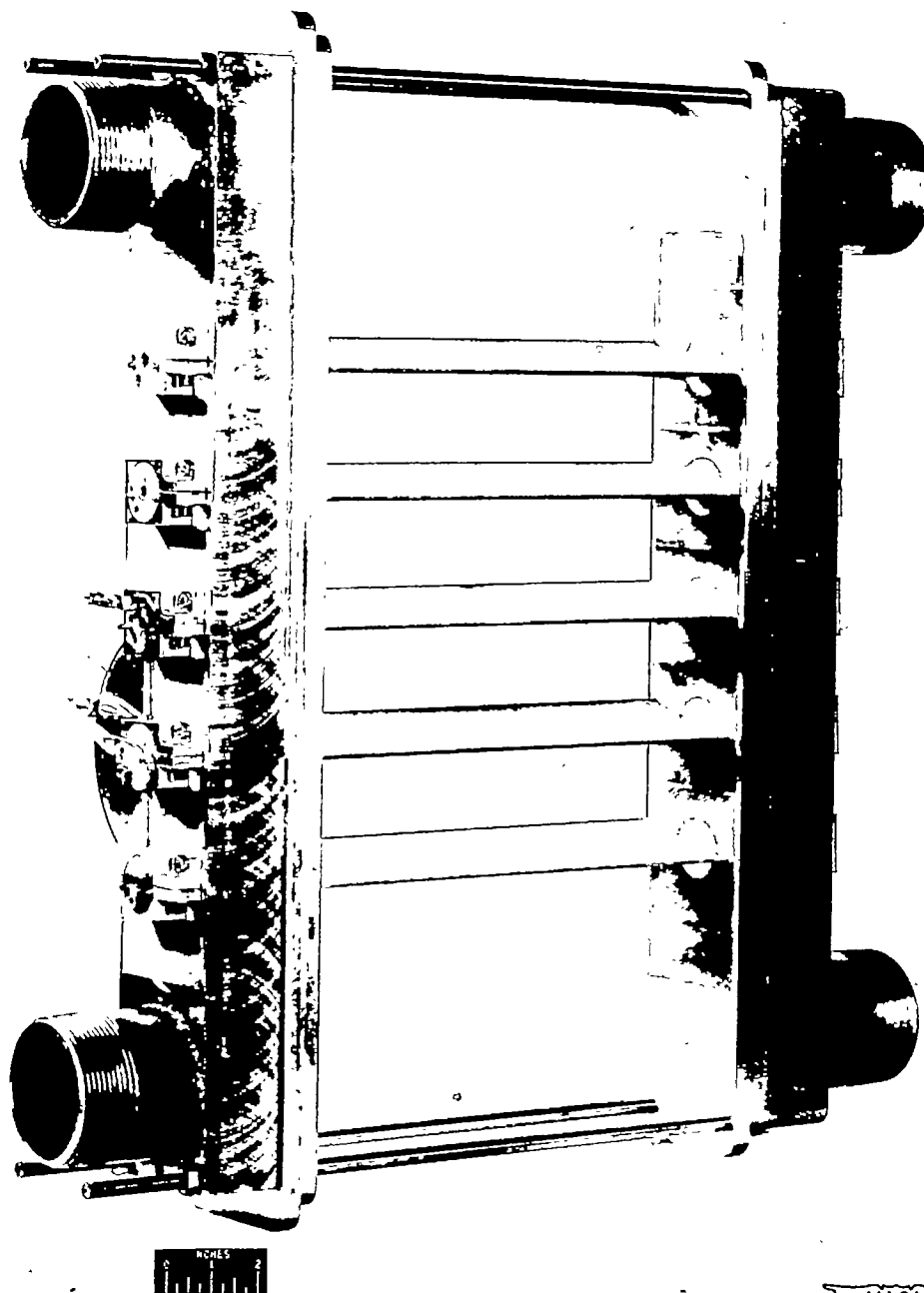
Figure 3. - Blades assembled in suction unit for introduction into tunnel. Porous
surfaces and manifold arrangement for removing air are shown.
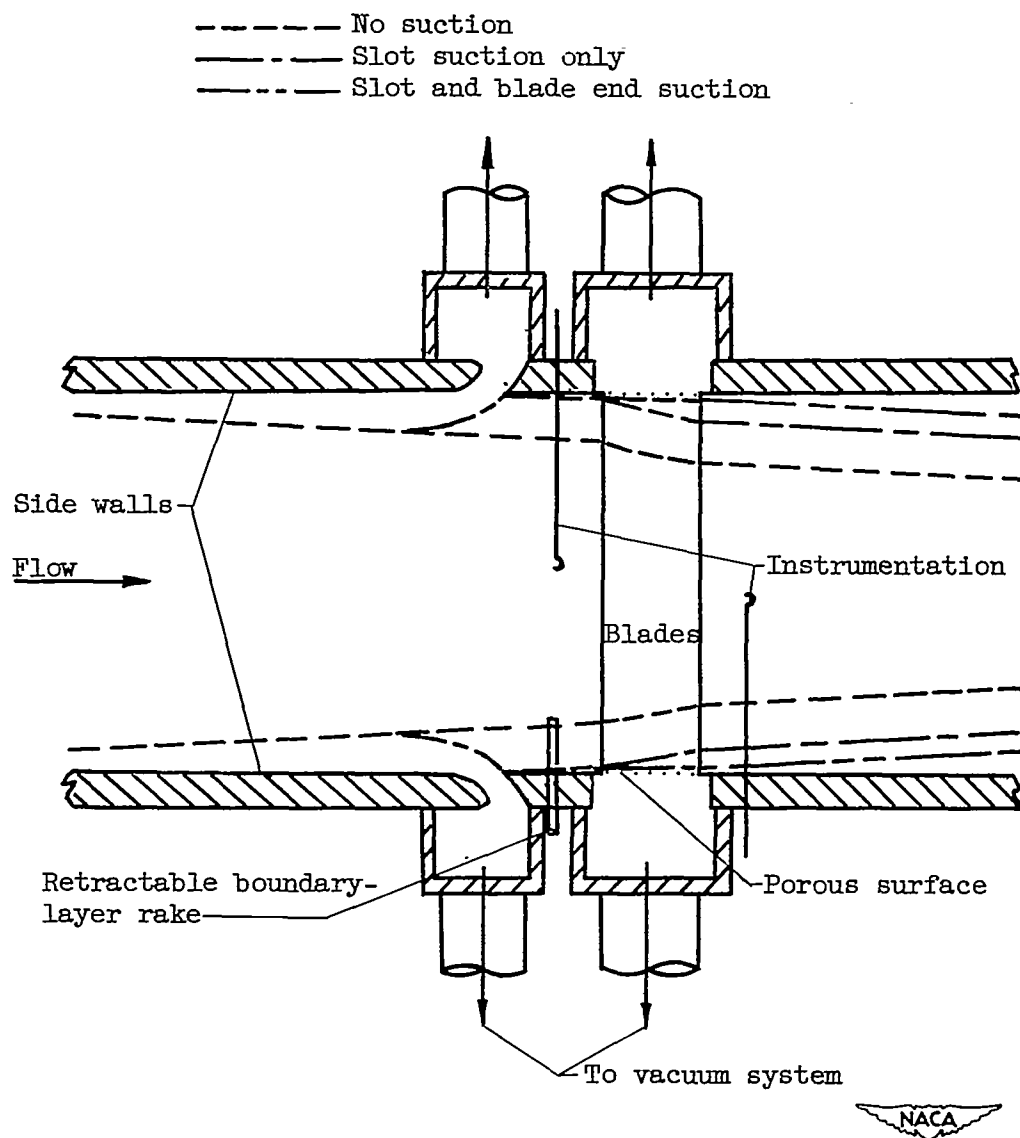
Figure 4. - Generalized tunnel plan representing manner of growth
of boundary-layer losses.

2472
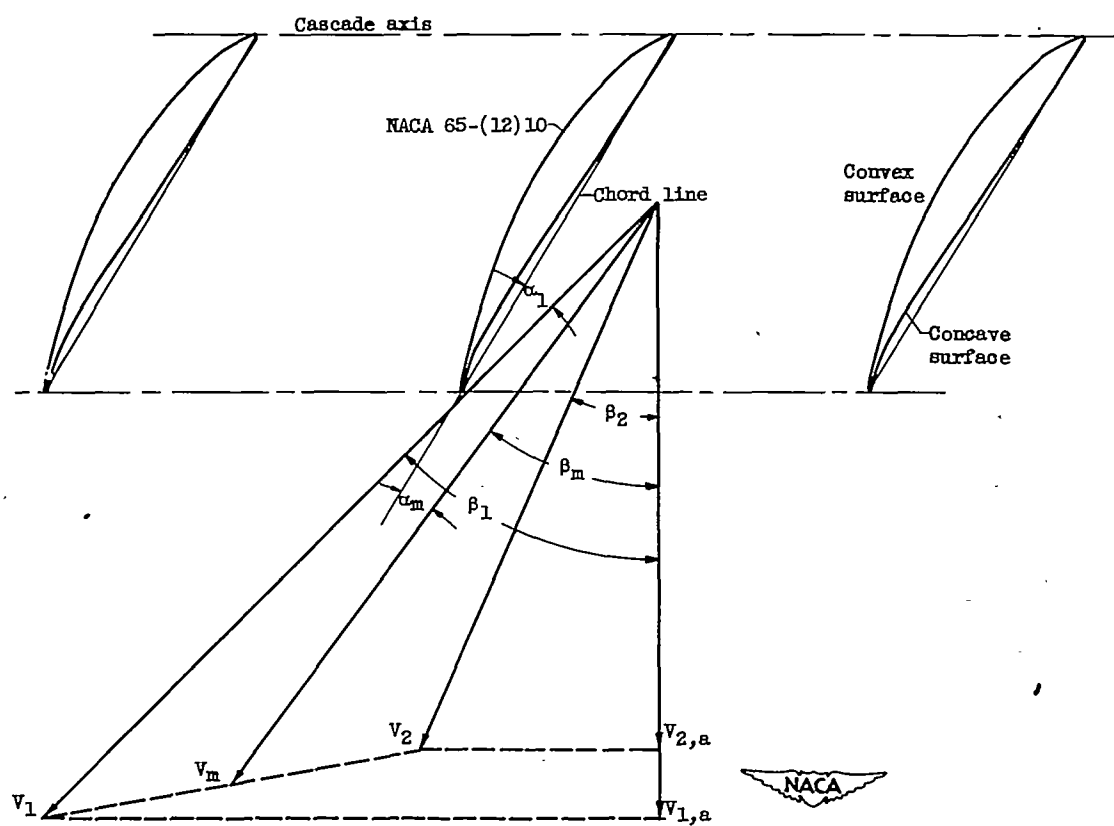
Figure 5. - Variation of velocity vectors across blade row.
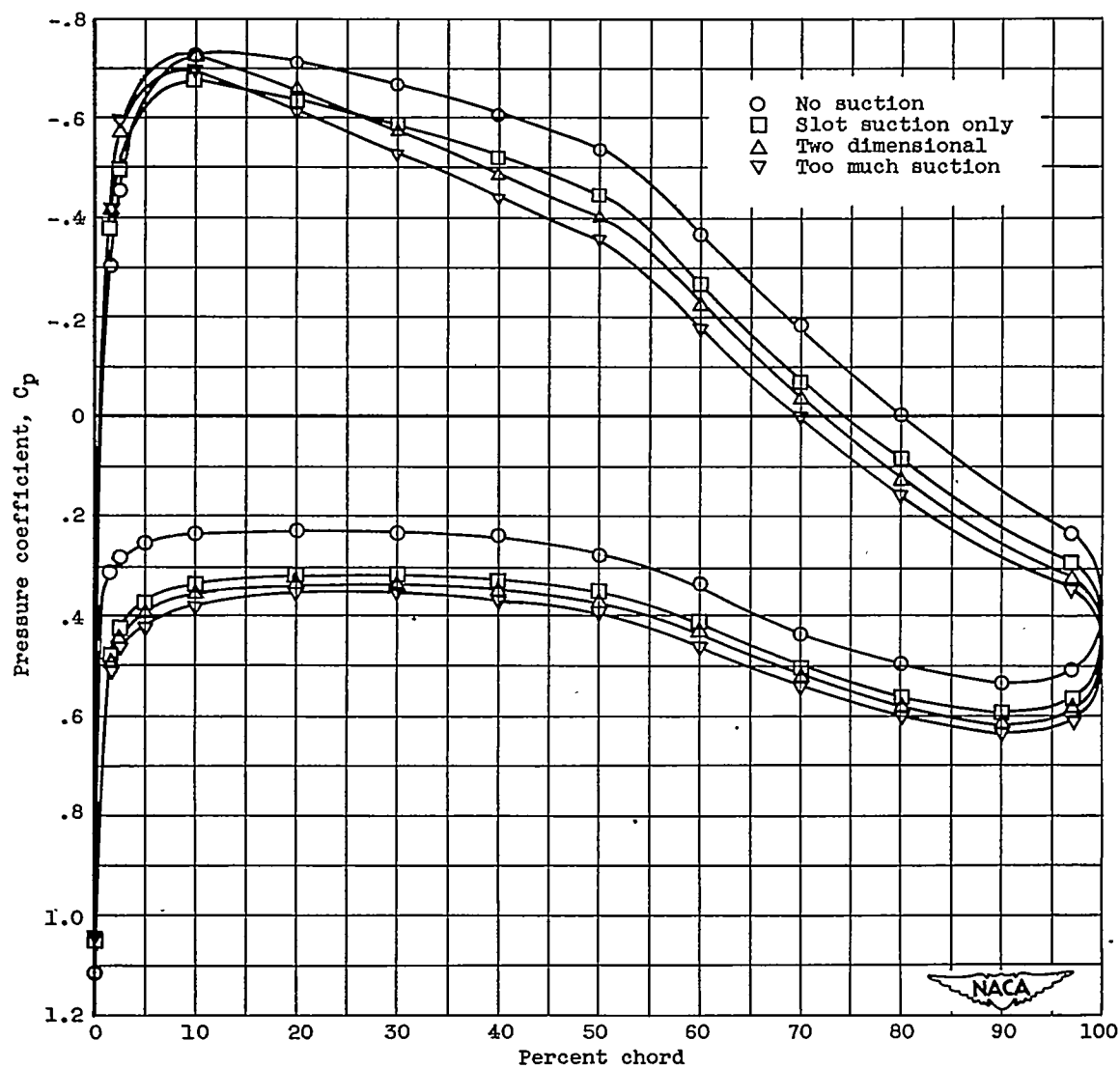
Figure 6. – Variation of pressure distribution at inlet Mach number of 0.4 when
various types and amounts of suction are employed.
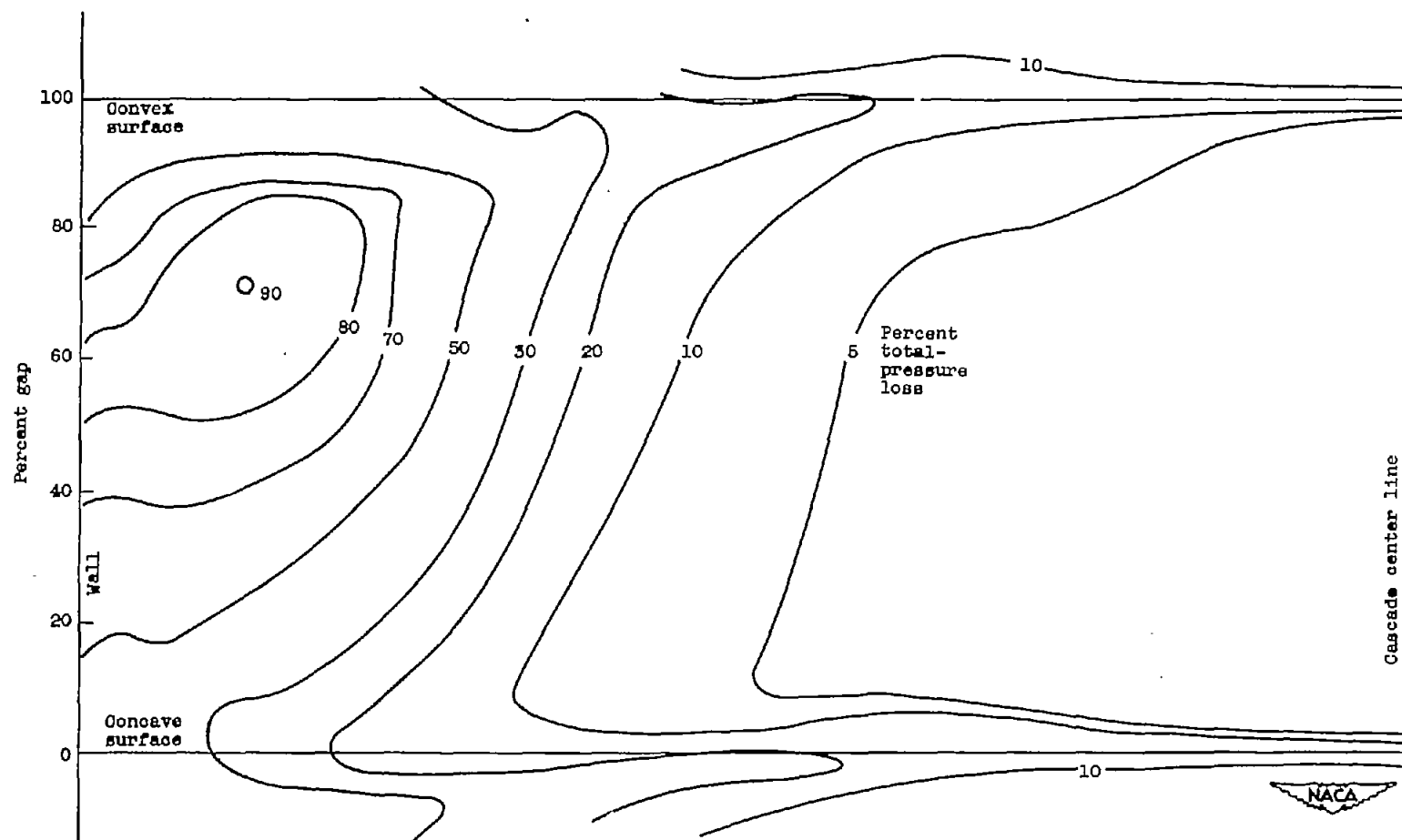
(a) No suction used.

Figure 7. - Total-pressure-loss parameter contour 1/2 chord downstream of blades. Inlet Mach number, 0.5.
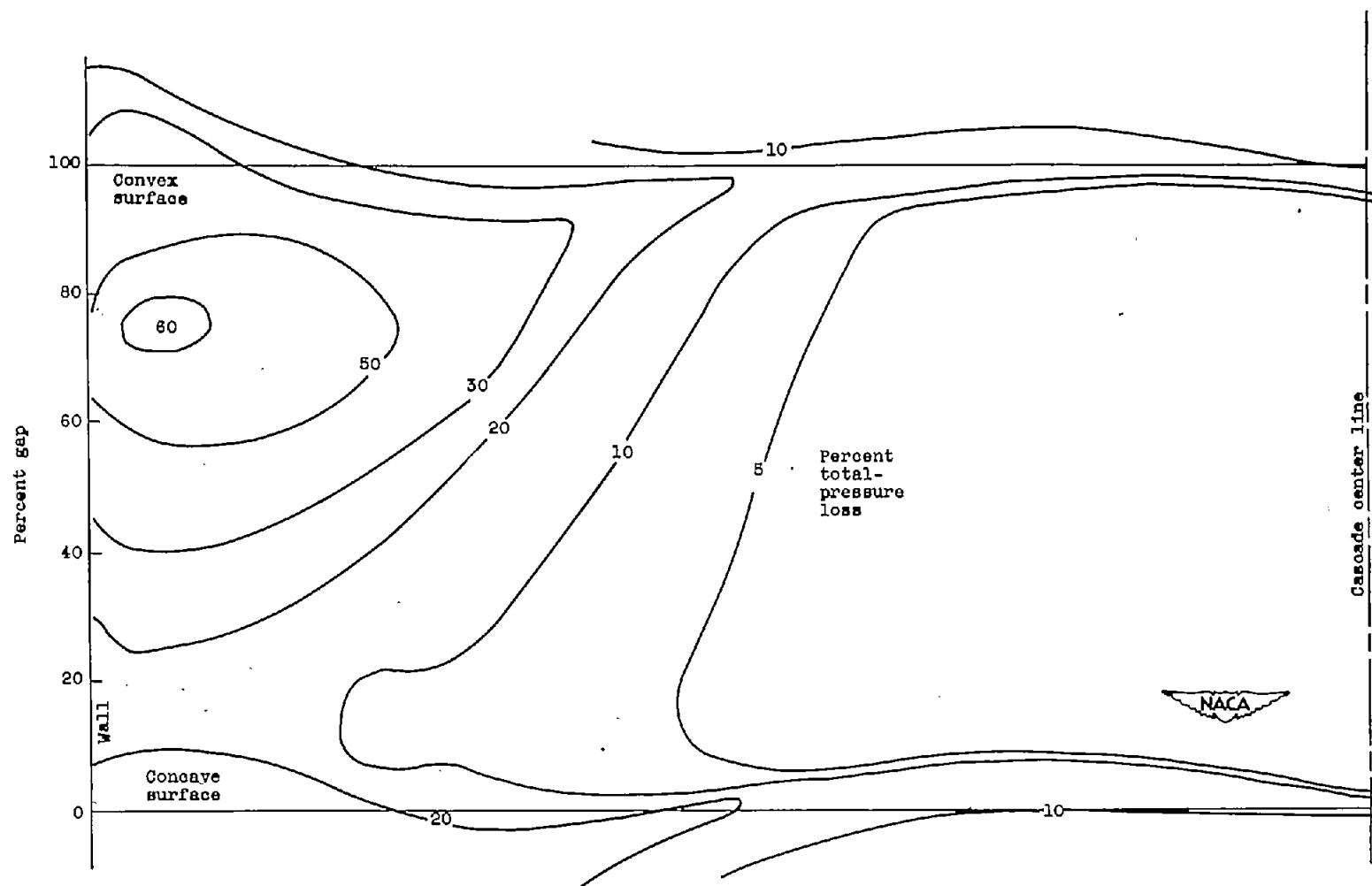
(b) Wall boundary layer controlled by suction through slot only.

Figure 7. - Continued. Total-pressure-loss parameter contour 1/2 chord downstream of blades. Inlet Mach number, 0.5.
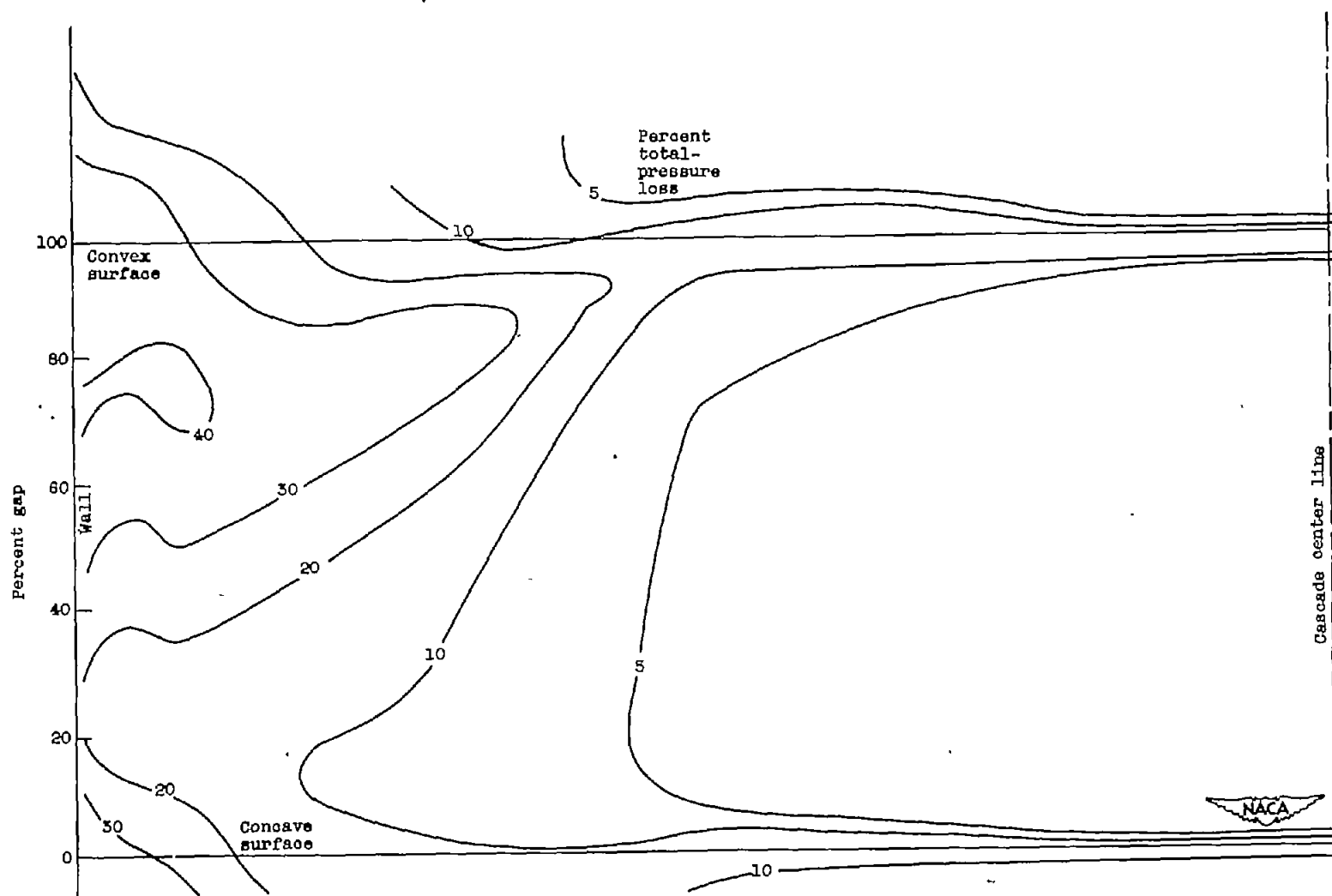
(c) Two-dimensionality satisfied.

Figure 7. - Concluded. Total-pressure-loss parameter contour 1/2 chord downstream of blades. Inlet Mach number, 0.5.
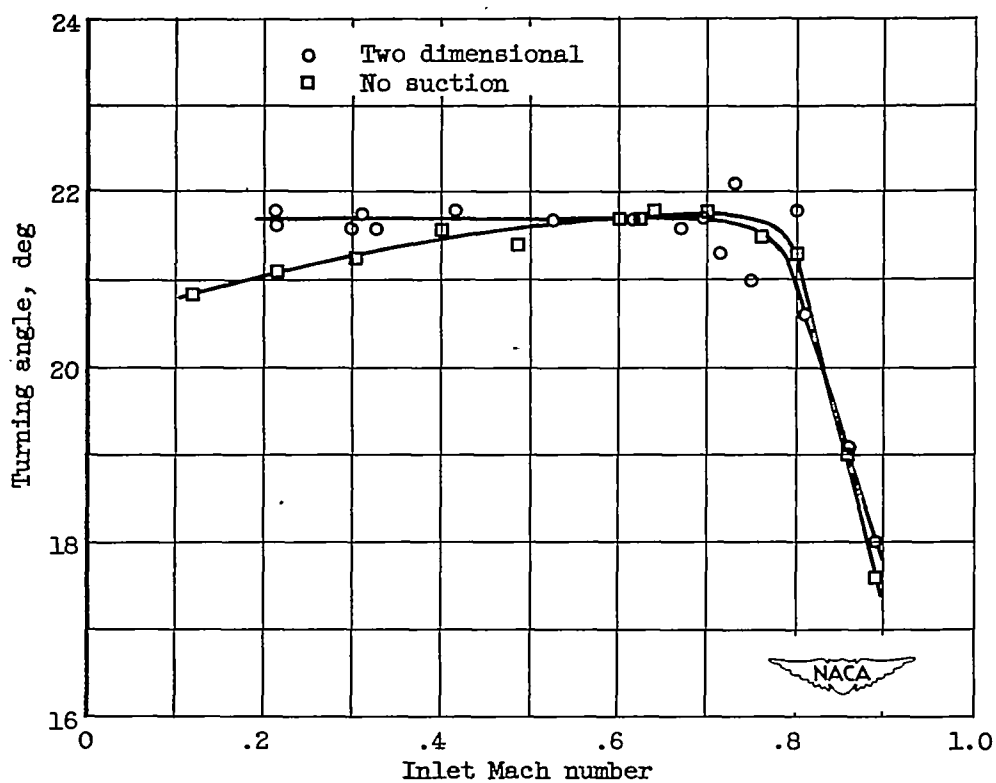
Figure 8. - Variation of turning angle with inlet Mach number.
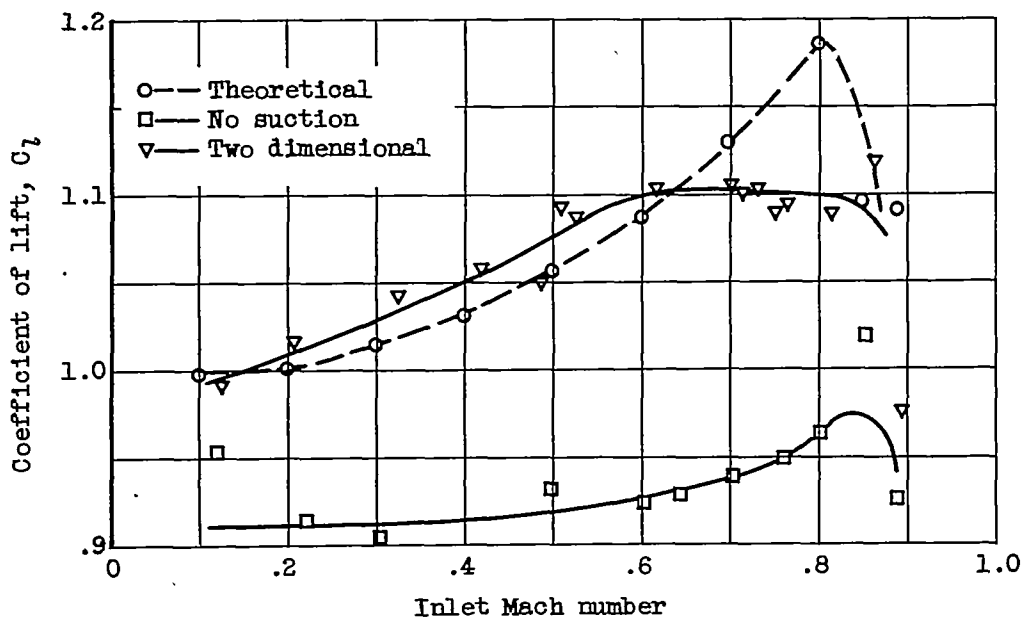
Figure 9. - Variation of C_l with inlet Mach number.
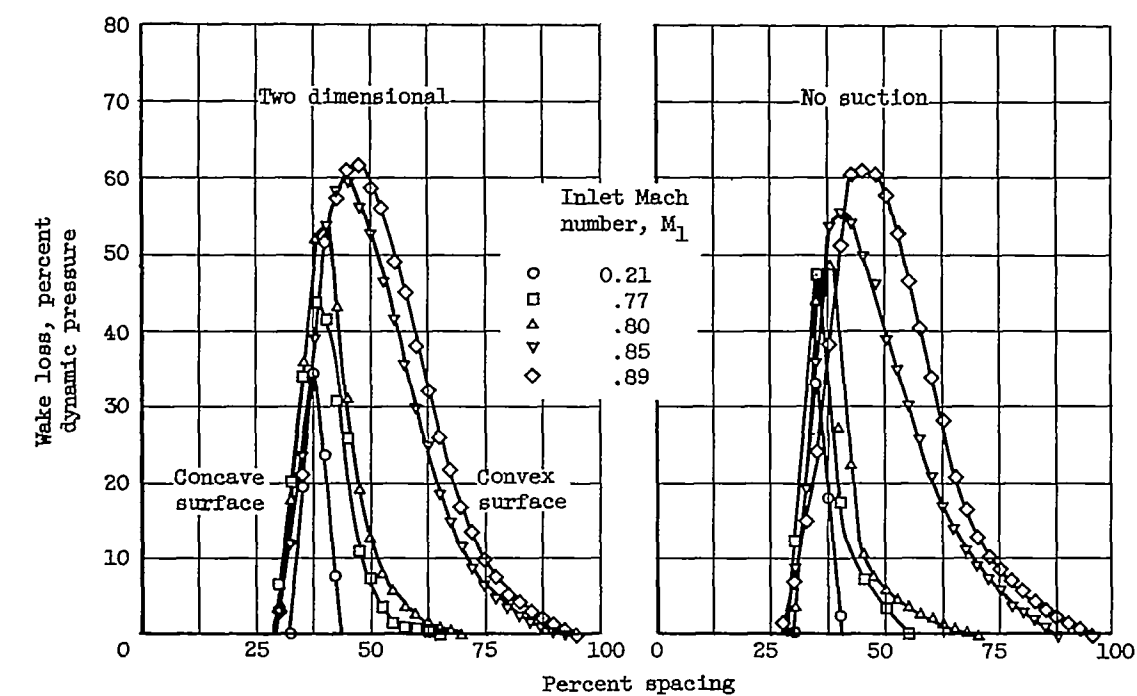
(a) Wake profiles 1/2 chord downstream of blades.
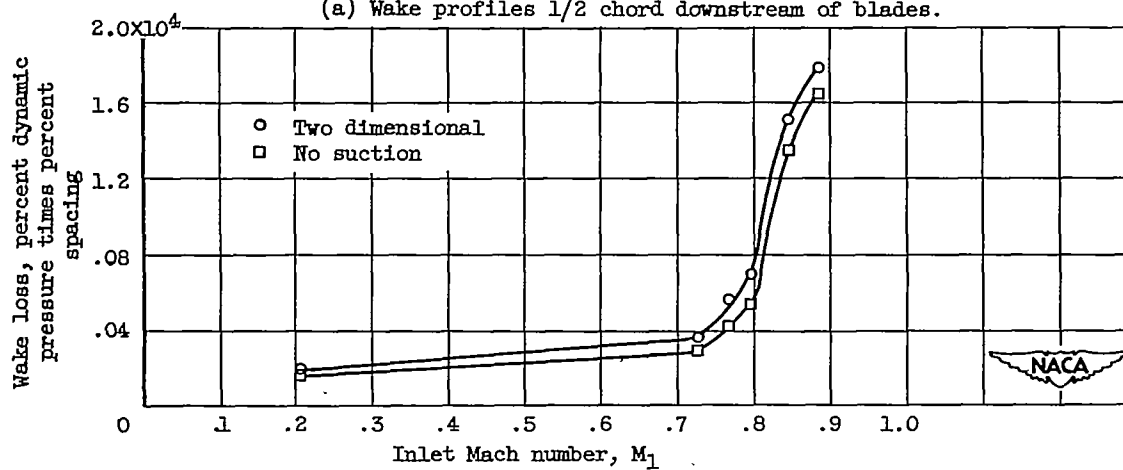
(b) Total wake deficiency, integrated percent dynamic pressure.

Figure 10. - Variation of blade wake measured on cascade center line with inlet Mach number.
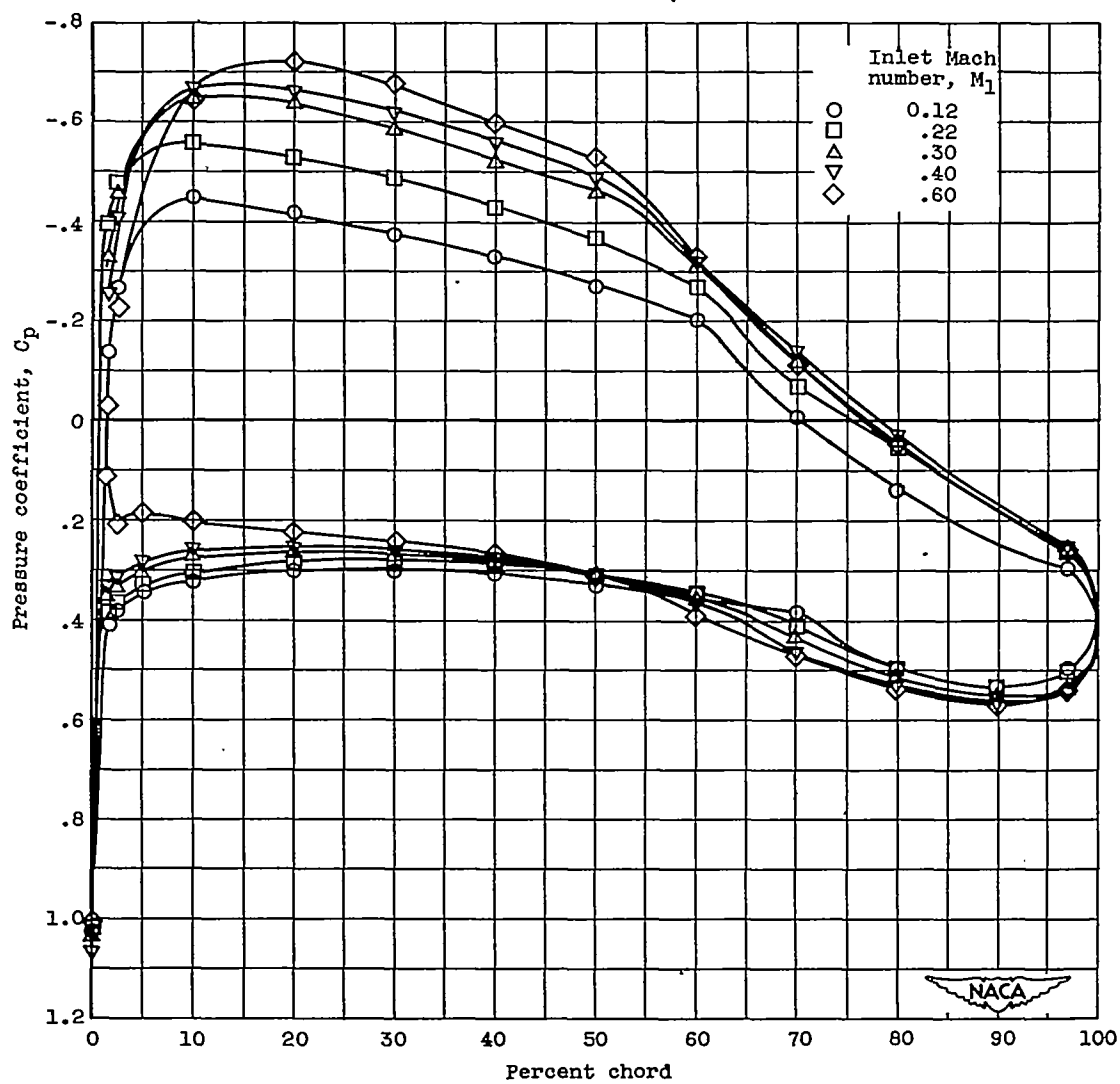
(a) Inlet Mach number ≦ 0.60.

Figure 11. - Pressure distribution variation with no suction.
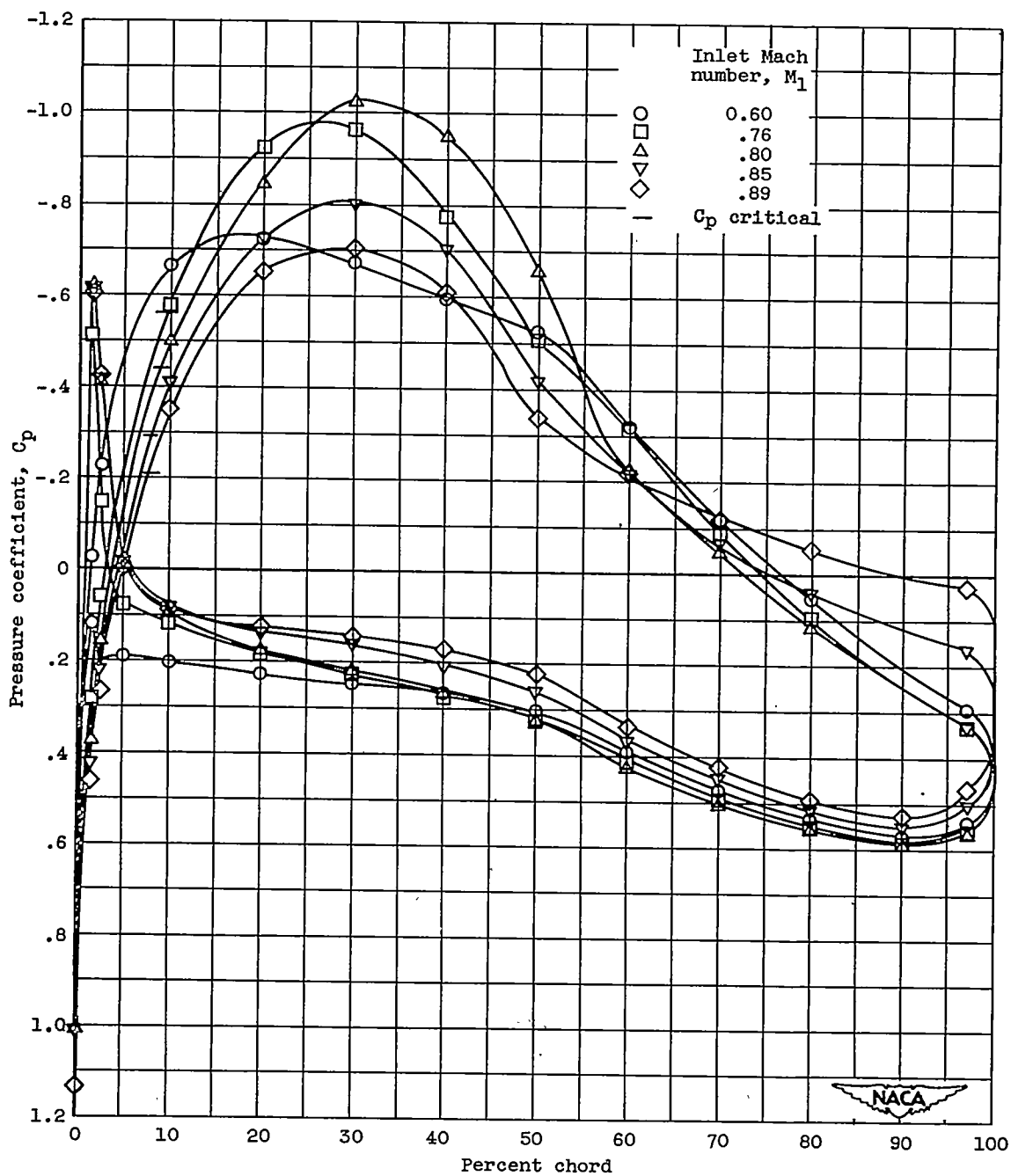
(b) $0.60 \leqq$ inlet Mach number $\leqq 0.89$.

Figure 11. - Concluded. Pressure distribution variation with no suction.
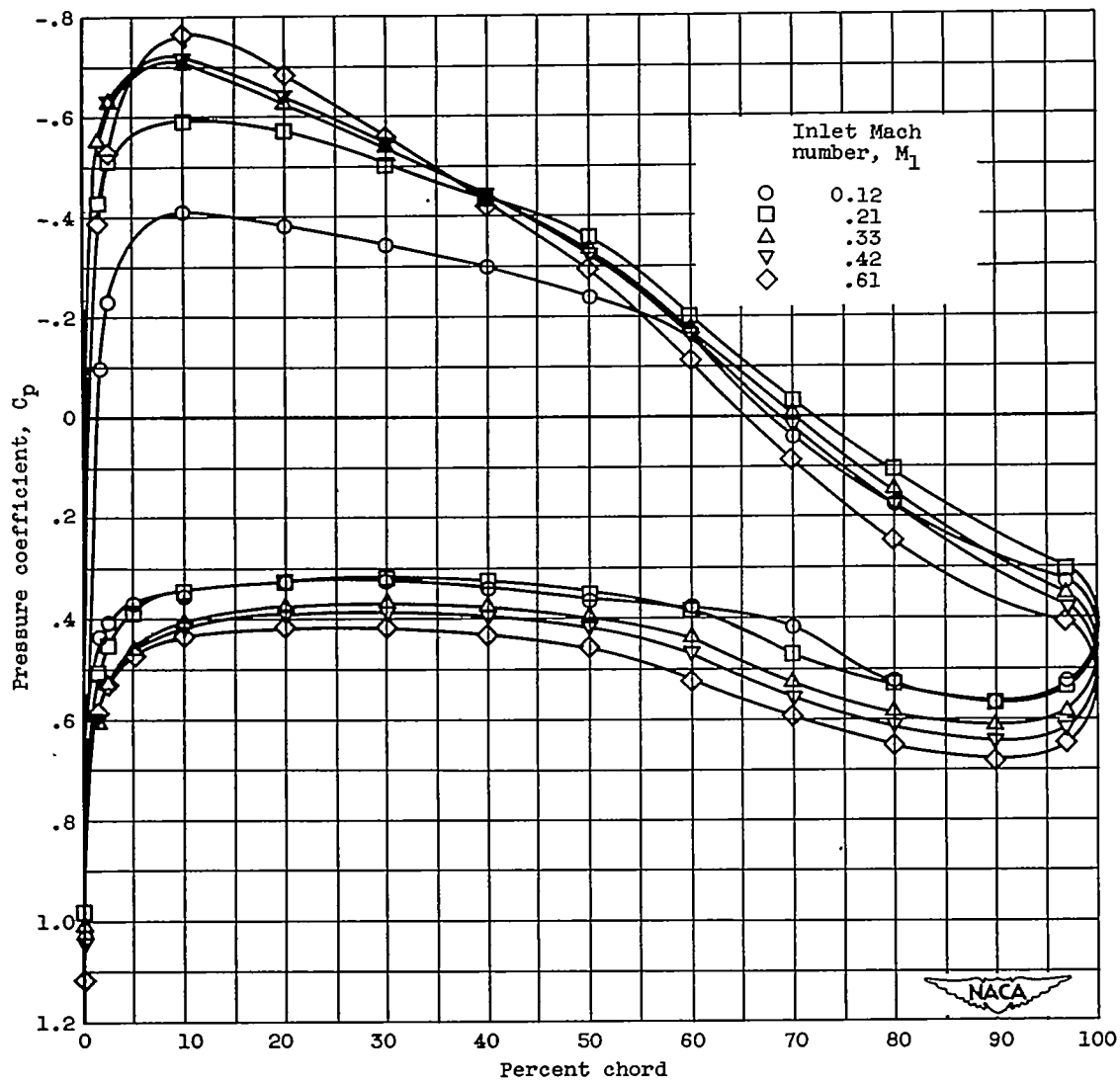
(a) Inlet Mach number $\leqq$ 0.61.

Figure 12. - Pressure distribution variation when two-dimensionality criterion is satisfied.

2472
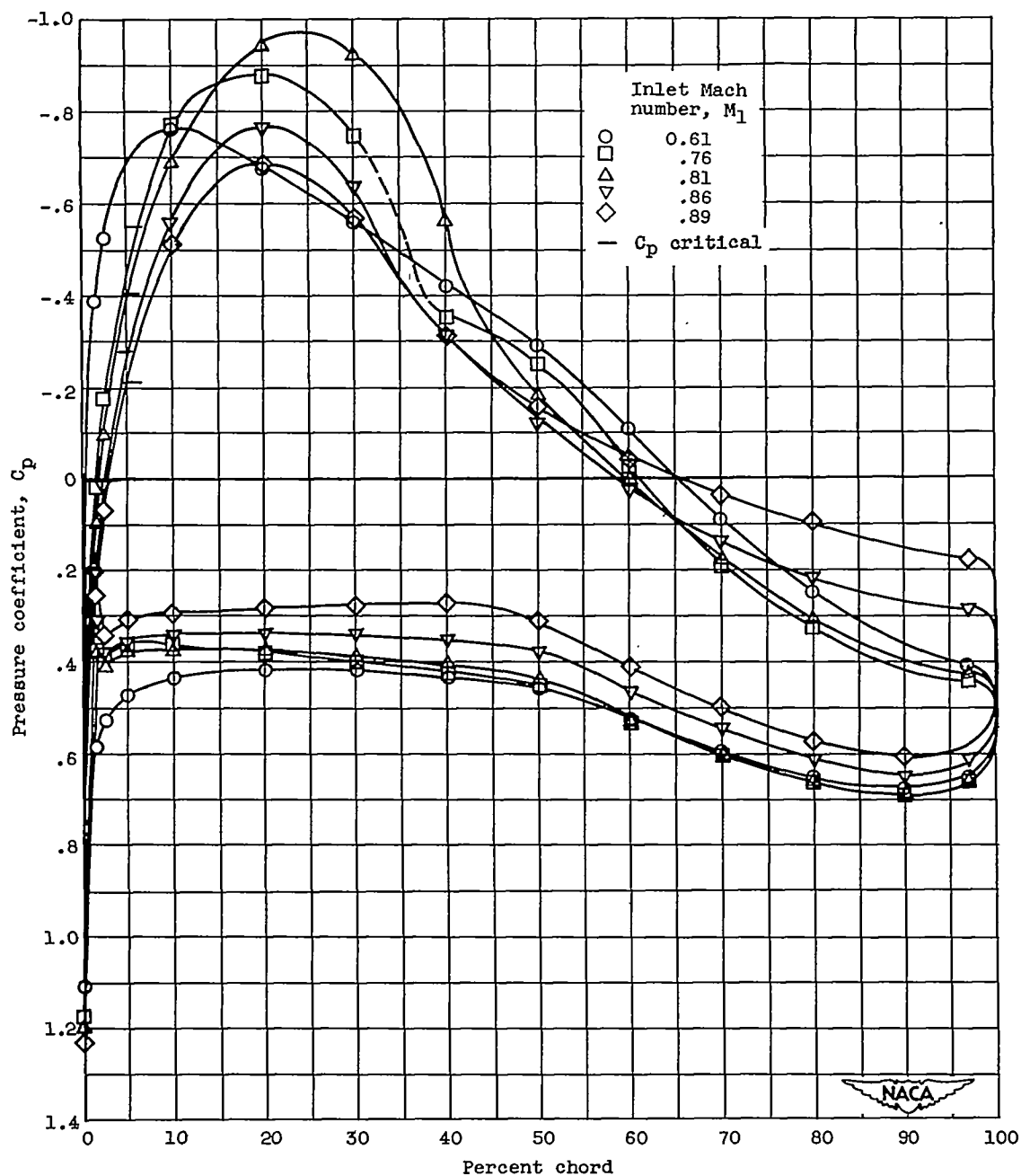
(b) 0.61 $\leqq$ inlet Mach number $\lesssim$ 0.89.

Figure 12. - Concluded.   Pressure distribution variation when two-dimensionality
criterion is satisfied.
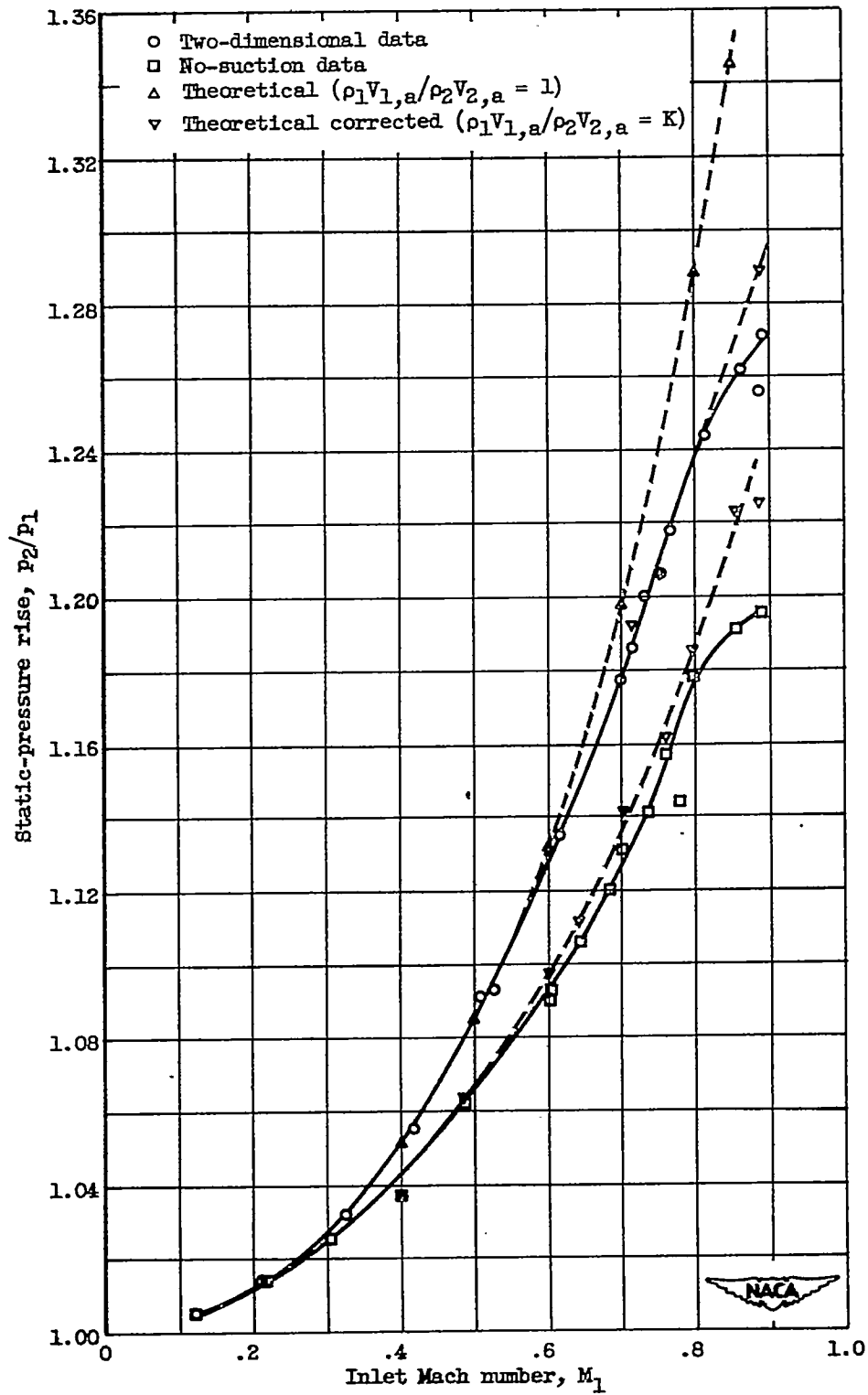
Figure 13. - Variation of static-pressure rise with Mach number. Correlation of data with theoretical values as corrected by contraction coefficient.

2472
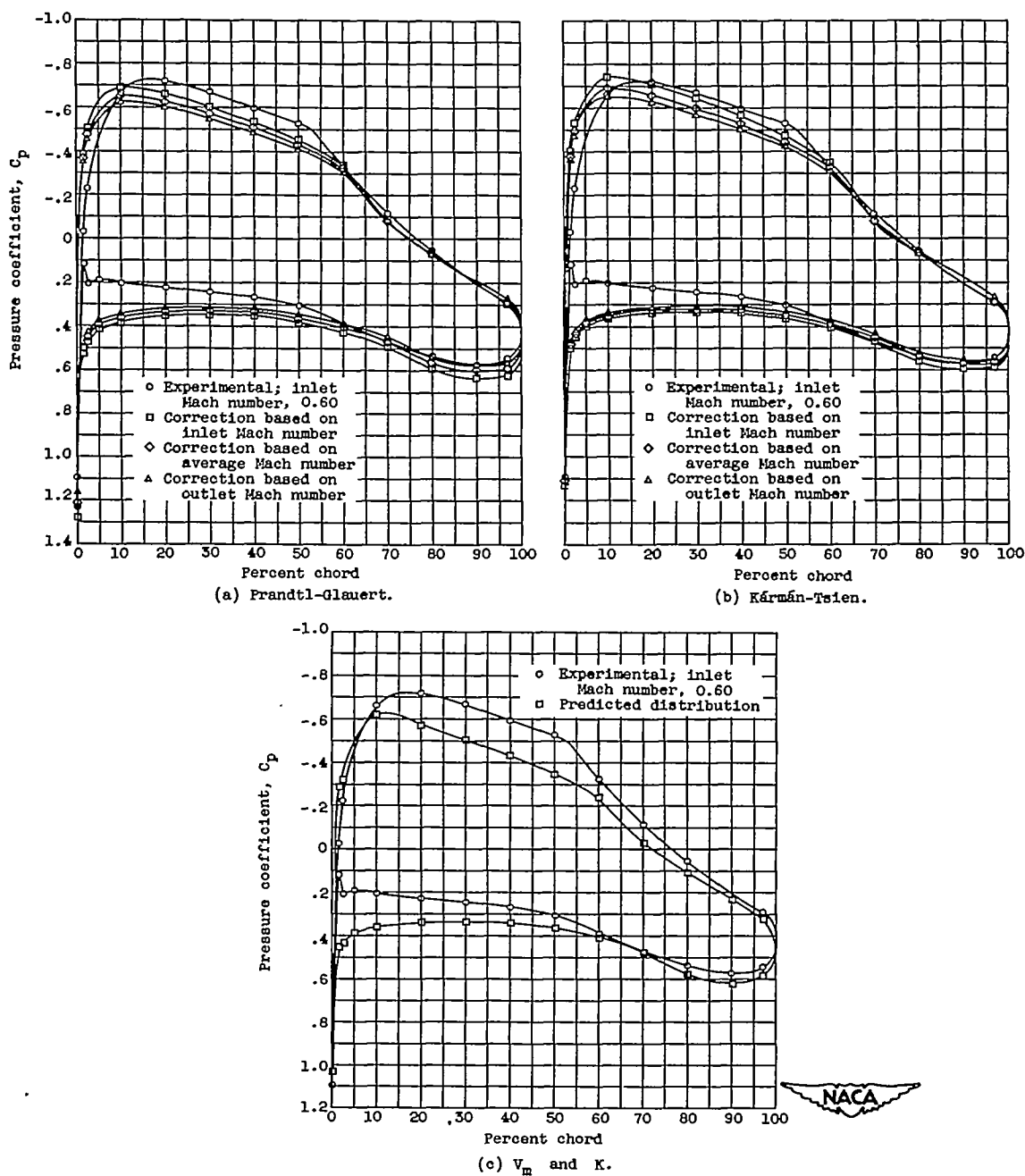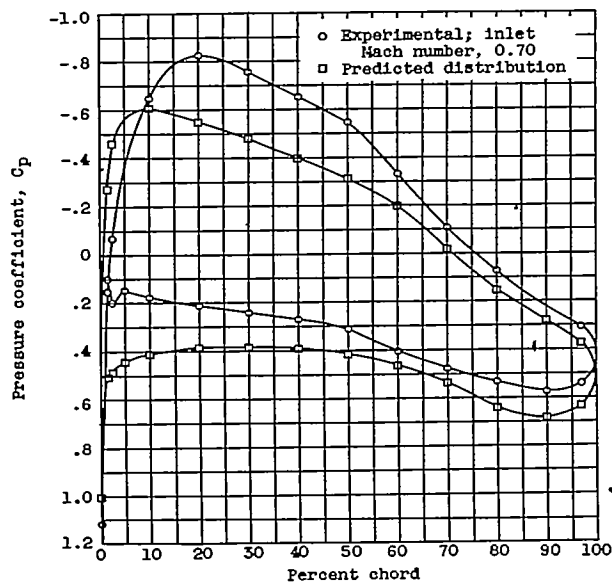

Figure 14. - No-suction condition; compressibility corrections applied to experimental pressure distribution at inlet Mach number 0.21 compared with experimental pressure distribution at inlet Mach number 0.60. σ_0, 0.89; $(\beta_1)_c$, 40.5°; maximum experimental M_b, 0.823.
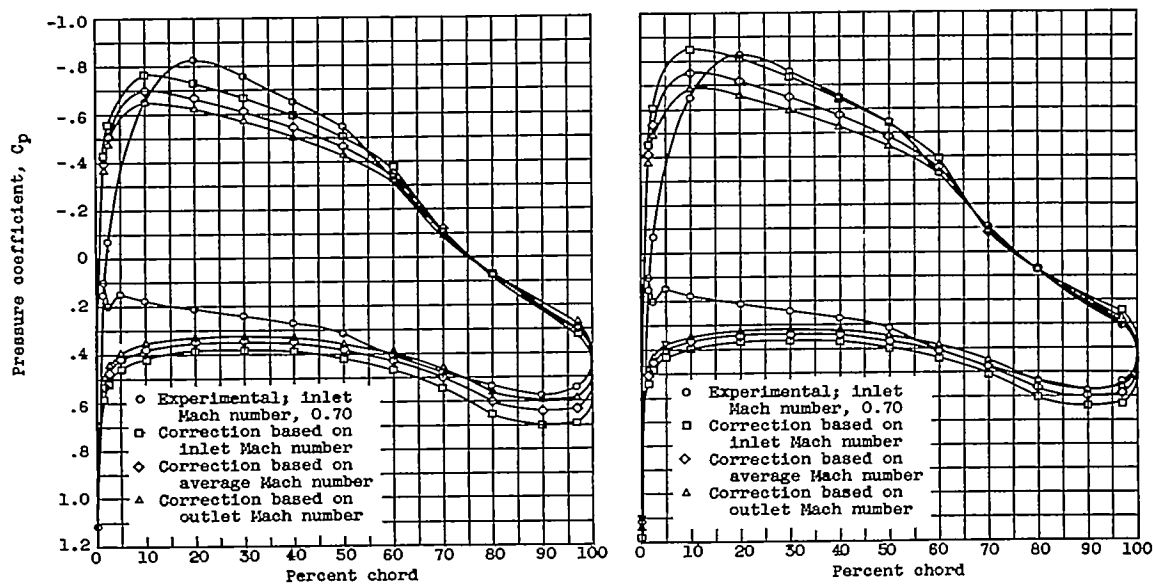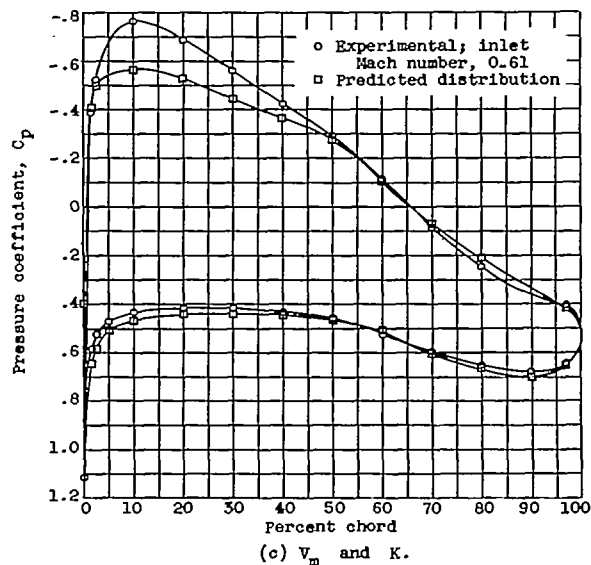
(a) Prandtl-Glauert.

(b) Kármán-Tsien.

(c) V_m and K.

Figure 15. - No-suction condition; compressibility corrections applied to experimental pressure distribution at inlet Mach number 0.21 compared with experimental pressure distribution at inlet Mach number 0.70. σ_o, 0.84; $(\beta_1)_c$, 38.9°; maximum experimental M_b, 1.007.

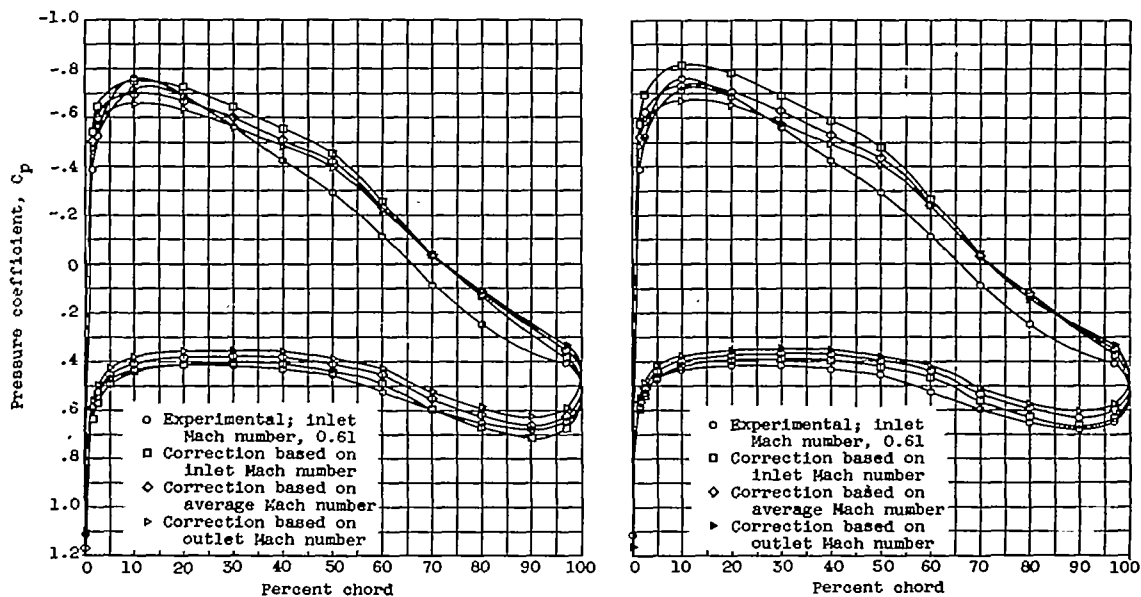(a) Prandtl-Glauert.
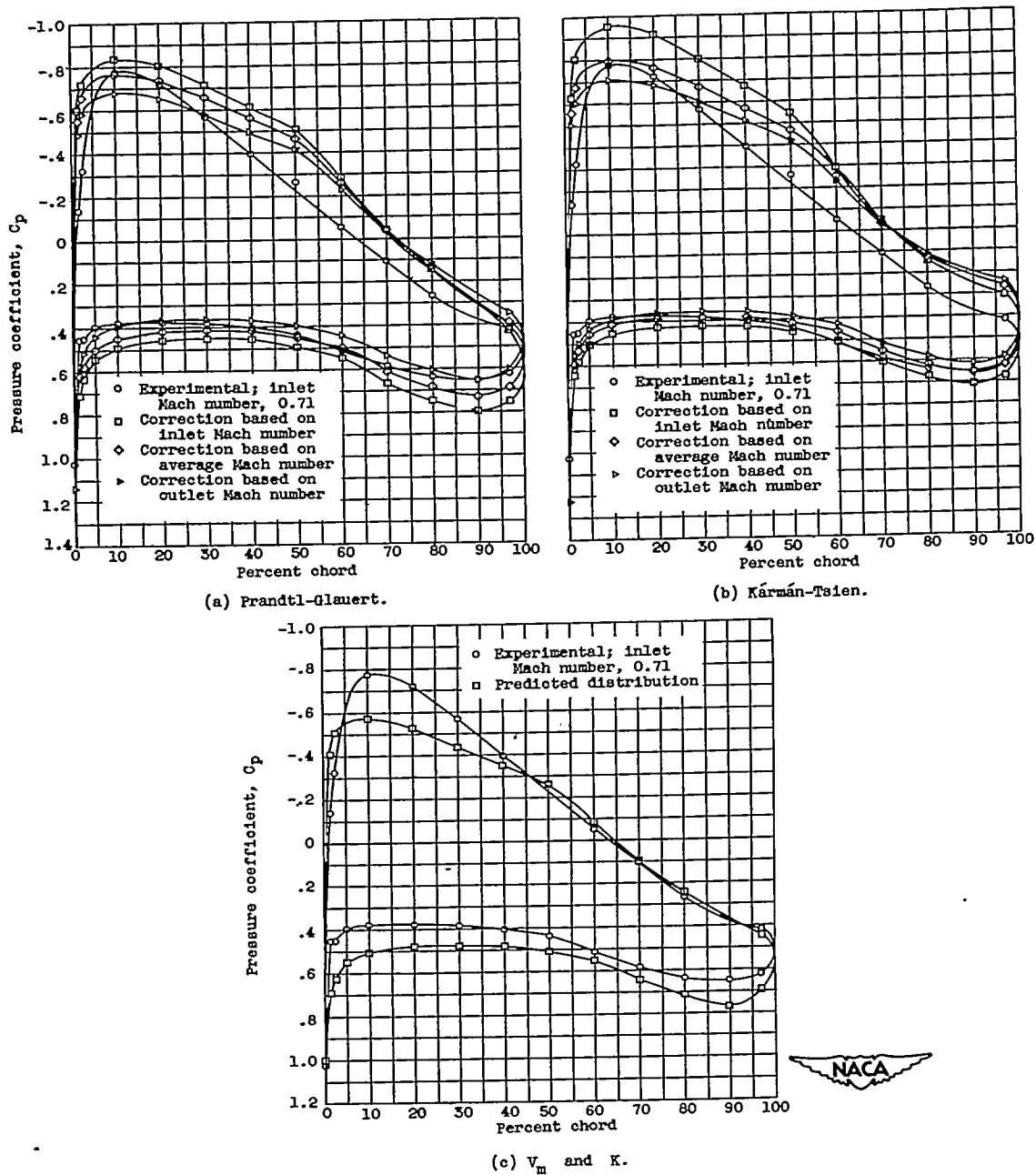
(b) Kármán-Tsien.

(c) V_m and K.

Figure 16. - Two-dimensional condition; compressibility corrections applied to experimental pressure distribution at inlet Mach number 0.21 compared with experimental pressure distribution at inlet Mach number 0.61. σ_c, 0.90; $(\beta_1)_c$, 40.8°; maximum experimental M_b, 0.859.

(a) Prandtl-Glauert.

(b) Kármán-Tsien.

(c) V_m and K.

Figure 17. - Two-dimensional condition; compressibility corrections applied to experimental pressure distribution at inlet Mach number 0.21 compared with experimental pressure distribution at inlet Mach number 0.71. σ_c, 0.85; $(\beta_1)_c$, 39.2°; maximum experimental M_b, 1.020.
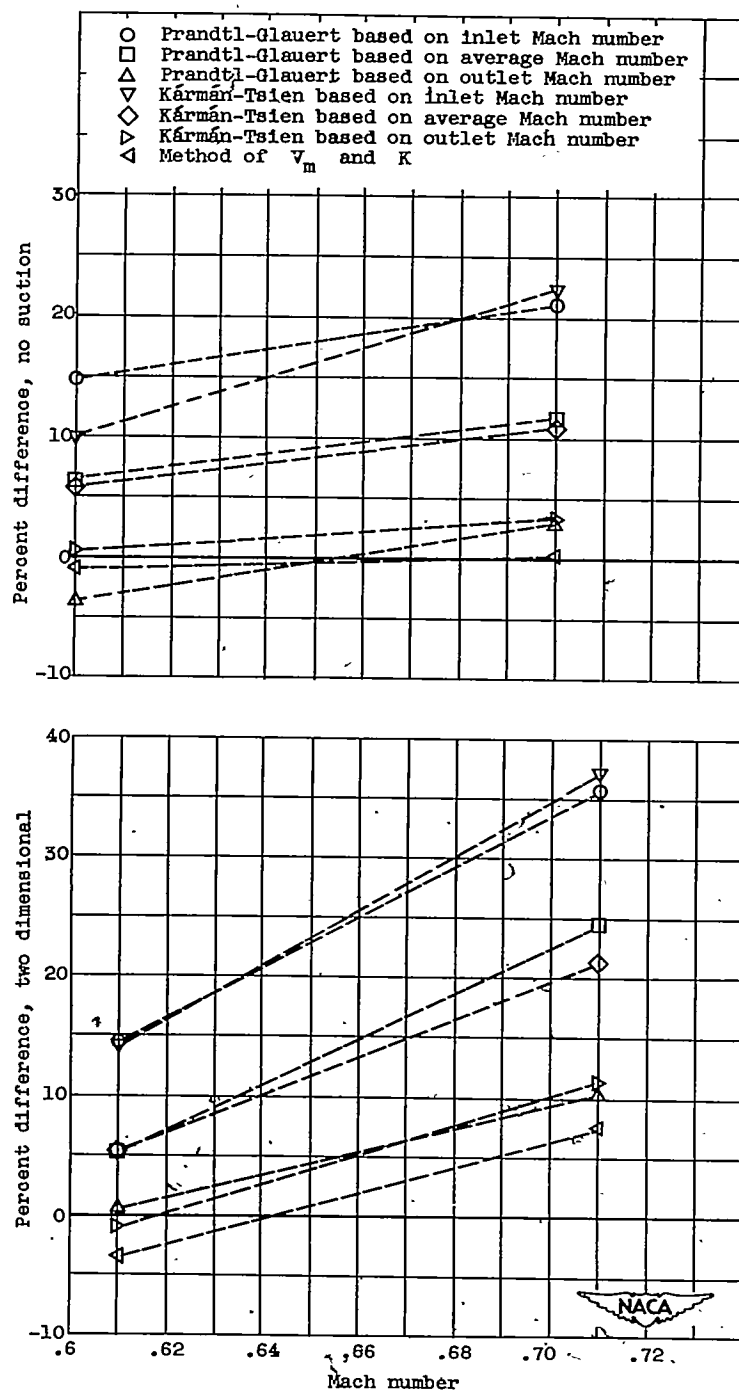
Figure 18. - Percentage difference in area of predicted and experimental pressure distributions plotted against Mach number.

$$\text{Percent difference} = \frac{\left(\int_0^c (p_p - p_u)dc\right)_{pred} - \left(\int_0^c (p_p - p_u)dc\right)_{exp}}{\left(\int_0^c (p_p - p_u)dc\right)_{exp}}$$